ACDIV-2013-16
December, 2013

Conceptual design study of a Storage Ring: First idea for a Mexican Light Source

A. Flores-Tlalpa

Abstract:

This technical report compares different Storage Ring lattices at linear optics level. These lattices are MAX IV (Sweden), SIRIUS (Brazil), NSLS II (U.S.), ESRF II (Europe), DIAMOND II (U.K.), SOLEIL (France) and ALBA (Spain). This is the starting point for an eventual new lattice design, which can be used for a possible future Mexican Light Project. These new designs are based on the 7BA cell of MAX IV (Max Lab) and the DBA cell of ALBA (CELLS). The magnetic lattice structure of MAX IV has one of the most innovative designs of the present time and allows a low emittance of the machine, a requirement that is currently in high demand by users of synchrotron light. However their main disadvantages are high costs and the limited space provided for insertion devices and radio frequency system. Meanwhile, the magnetic lattice structure of ALBA has the advantage of providing a reduced cost and a larger free space for insertion devices, although the emittance is almost twice the one based on the MAX IV lattice. Based on the 7BA cell such as of the MAX
IV facility, the results with the smallest circumferences are: a circumference C = 343m and a horizontal emittance "x = 1:2 nm_rad. Based on the ALBA DBA cell, these parameters are: C = 336 m and "x = 2:3 nm_rad. In all cases the beam energy has fixed to 3 GeV, which is the currently value of the ALBA and MAX IV facilities. Since currently the Mexican project does not have specificc requirements and budget, this report also presents other solutions with larger circumferences.

Accelerator Division
Alba Synchrotron Light Source
Ctra. BP 1413 Km. 3,3
08290 Cerdanyola del Valles, Spain

Conceptual design study of a Storage Ring: first idea for a Mexican Light Source

A. Flores-Tlalpa, ALBA-CELLS, Cerdanyola, Spain.

January 2014

Abstract

This technical report compares different Storage Ring lattices at linear optics level. These lattices are MAX IV (Sweden), SIRIUS (Brazil), NSLS II (U.S.), ESRF II (Europe), DIAMOND II (U.K.), SOLEIL (France) and ALBA (Spain). This is the starting point for an eventual new lattice design, which can be used for a possible future Mexican Light Project. These new designs are based on the 7BA cell of MAX IV (Max Lab) and the DBA cell of ALBA (CELLS). The magnetic lattice structure of MAX IV has one of the most innovative designs of the present time and allows a low emittance of the machine, a requirement that is currently in high demand by users of synchrotron light. However their main disadvantages are high costs and the limited space provided for insertion devices and radio frequency system. Meanwhile, the magnetic lattice structure of ALBA has the advantage of providing a reduced cost and a larger free space for insertion devices, although the emittance is almost twice the one based on the MAX IV lattice. Based on the 7BA cell such as of the MAX IV facility, the results with the smallest circumferences are: a circumference $C = 343$ m and a horizontal emittance $\varepsilon_x = 1.2$ nm·rad. Based on the ALBA DBA cell, these parameters are: $C = 336$ m and $\varepsilon_x = 2.3$ nm·rad. In all cases the beam energy has fixed to 3 GeV, which is the currently value of the ALBA and MAX IV facilities. Since currently the Mexican project does not have specific requirements and budget, this report also presents other solutions with larger circumferences.

Contents

1 Introduction

Today synchrotron light sources are multidisciplinary centers where scientists from different areas of knowledge carry out their research projects, the biology, chemistry, medicine, materials science and nanoscience are just some of these areas. Two factors have been decisive for the popularity enjoyed by synchrotrons, first, the unique properties of synchrotron radiation, such as wide-energy tunability, high brightness, extreme collimation, polarization, and time structure; and second, the study techniques that have been developed since the early days of their use in the 1960s. The modern synchrotron light sources (third generation) are the products of several generations of advances in light source technology.

In particular, medium energy light source ($\sim$ 2.5 to 3.5 GeV), occupying the middle ground between low energy and high energy storage rings, have rapidly gained popularity in recent times. These facilities are distinguished by having a combination of high operating current, low beam emittance, and advanced insertion devices (ID) technology; and their utility has been extended by technological progress in many areas. Among these, progress in undulator technology is especially important, as it boosts the bright radiation output of the medium energy machines into the most heavily used 5 to 20 keV range.

Some medium energy light source are currently operating (e.g. ALBA, SOLEIL and DIAMOND) and many others are either in design (e.g. SIRIUS) or under construction (e.g. MAX IV and NSLS II) around the world. In Latin America there is only one synchrotron, the LNLS in Brazil, and the new Brazilian light source (SIRIUS) is currently in planning. The vast majority of these machines are in more developed countries, such as Germany, U.S. and Japan. However, most of top 15 economies of the world have at least one synchrotron, except Mexico.

Because the development of a country is closely linked to its development in science and technology, diverse voices, arising both scientists and government officials, have raised the building of a synchrotron light source in Mexico. Even some Mexican researchers have presented proposals in this regard, see references [1]-[3], due to growing interest of the users of such facilities and the scientific community that is interested in the development of the accelerator physics. Undoubtedly if this megaproject is done, it will be a very important engine of the development of science and technology in Mexico, plus it has the potential to boost the development of specific industries. However, to date the technical specifications of the eventual Mexican light source have not yet been fixed.

In this report, some preliminary studies that may eventually serve as a starting point for the Mexican synchrotron light source are presented. Specifically, these studies are focused on the storage ring of the machine, where the electron beam is circulated to produce synchrotron radiation. Because the technical specifications of the machine does not exist, a comparison between some medium energy light sources (2.75 and 3 GeV) was performed, which also included a high energy facility (6 GeV). The medium energy facilities are ALBA (Spain), SOLEIL (France), DIAMOND (U.K.), SIRIUS (Brazil), MAX IV (Sweden) and NSLS II (U.S.), while ESRF (France) was chosen as the high energy facility. This allowed to choose two storage ring designs of medium energy (3 GeV), namely, the ALBA and MAX IV designs, which were subsequently adapted so that they can serve as seed designs for the synchrotron light source of Mexico.

Should be noted that all studies presented here were performed essentially in the linear approximation of beam dynamics, or also called linear optics.

Many and diverse factors must be taken into account in the design of a synchrotron, from my perspective, two of the most important are the user needs and the budget allocated. According to international experience, a requirement that users generally demand is that the emittance of the electron beam in the storage ring should be small, on the order of nanometers or less (subnanometers), so that the photon beam produced has a high brilliance. On the other hand, the cost must be contained, which limits among other things the storage ring size and the budget of the technology that will be used. A restricted size of the storage ring is a limitation to reduce emittance, because the conventional way to reduce the emittance is increase the number of dipole magnets, which inevitably increases the size of the storage ring circumference. Therefore, a feasible design must strike a balance between user requirements and budget constraints.

It is noteworthy that the MAX IV storage ring has one of the most innovative lattice designs allowing a low emittance of the electron beam, however, its high cost and reduced space for free straight sections are major disadvantages. By contrast, the ALBA storage ring has the advantage of providing a reduced cost and a large space for free straight sections, but its emittance is much bigger. Therefore, these medium energy facilities have the precise features that must be balanced (high performance vs contained cost) to obtain a feasible design.

The comparison between the storage ring lattices that were selected is presented in Section 2. And in Section 3, I present two pairs of lattice designs for a storage ring of 3 GeV energy. Each pair consists of two lattices with similar circumferences, one based on the MAX-IV storage ring design and the other based on ALBA design. I worked in two circumference sizes for that, this work could offer different solutions to the conflict between the size of the storage ring and the emittance.

2 Modern Light Sources

ALBA, SOLEIL, DIAMOND, MAX IV, NSLS II, SIRIUS and ESRF are the 3rd generation light sources that were selected to analyze and compare the designs of their storage rings, focusing on the magnetic structure of the lattices. Only one of these facilities, ESRF, operates at high energy, the others are medium energy light sources. At present, SIRIUS is in the planning, while NSLS II and MAX IV are under construction; ALBA, SOLEIL, DIAMOND and ESRF are light sources currently operating. However, the ESRF facility is currently in its first upgrade phase and a second phase is planning, on the other hand, studies are underway to upgrade the SOLEIL and DIAMOND facilities. The comparison is performed using the upgrade studies of DIAMOND and ESRF(in its second phase, ESRF II), while for SOLEIL the current lattice is used.

The main parameters of the storage ring of said facilities are given in Tables 2.1 and 2.2. More detail descriptions are given below, however, for now it is useful to pay attention to the following parameters: the circumference length and the horizontal emittance. The larger circumferences are those of the ESRF II and NSLS II machines, while ALBA is the light source with the shortest circumference; thus, the storage ring designs of the first two facilities are not the cheapest options, but the ALBA design yes it is. Now, between the lattices

Parameter	ESRF II	SOLEIL	MAX IV	ALBA	Units
Circumference	844	354.1	528	268.8	m
Percentage of straight sections	23	45	28	36	%
Energy	6.04	2.75	3	3	GeV
Current	200	430	500	400	mA
Horizontal emittance	0.15	3.91	0.33	4.4	nm.rad
Magnetic lattice structure	7BA	DBA	7BA	DBA	–
Number of cells	32	16	20	16	–
Bending angle of cell	11.25	22.5	18	22.5	deg
RF frequency	352	352.2	99.9	500	MHz
Harmonic number	991	416	176	448	–
Revolution frequency	3.554	0.847	0.568	1.116	MHz
Revolution period	0.281	1.180	1.761	0.896	μs

Table 2.1. Main parameters for the storage rings of ESRF II, SOLEIL, MAX IV and ALBA.

Parameter	NSLS II	DIAMOND upgrade	SIRIUS	Units
Circumference	792	561.6	518.3	m
Percentage of straight sections	25	25	25	%
Energy	3	3	3	GeV
Current	500	300	500	mA
Horizontal emittance	2.1	2.50	0.28	nm.rad
Magnetic lattice structure	DBA	DDBA	5BA	–
Number of cells	30	24	20	–
Bending angle of cell	12	15	18	deg
RF frequency	499.5	500	499.8	MHz
Harmonic number	1300	936	864	–
Revolution frequency	0.384	0.534	0.578	MHz
Revolution period	2.603	1.872	1.729	μs

Table 2.2. Main parameters for the storage rings of NSLS II, DIAMOND upgrade and SIRIUS.

of SOLEIL, DIAMOND (upgrade), MAX IV and SIRIUS, those with the smaller emittances are the MAX IV and SIRIUS lattices. As is mentioned above, MAX IV is currently in construction and SIRIUS yet is in the planning, so that the Swedish project is the most reasonable choice of a light source with a competitive emittance today. Another advantage of MAX IV is that much of its information can be easily obtained, including the simulation programs of the lattice dynamics, which were very useful in this work.

Then, the designs of the MAX IV and ALBA storage rings are the most sensible choices as the foundations for design of the Mexican project. For this reason, their descriptions, that are given below, are more detailed, whereas the description of the other facilities are brief.

The free straight sections of storage ring are essentials in a 3$^{\text{rd}}$ generation synchrotron light source, because in these are installed the insertion devices, and the injection and radio-frequency systems. Since the circumferences have very different lengths, the percentage of free straight sections in a storage ring is a more useful parameter for comparison. In this regard, the ALBA lattice is better than the MAX IV lattice, with 36% (97.6 m) and 28% (142 m) of free straight sections, respectively, but the lattice SOLEIL is the best all with 45% (160.8 m).

2.1 NSLS II

At Brookhaven National Laboratory (U.S.) the new synchrotron light source NSLS II is being built. This 3$^{\text{rd}}$ generation facility will have a storage ring of 780 meters, the energy, current (in multibunch operation mode) and horizontal emittance of the electron beam will be, respectively, 3 GeV, 500 mA and 2.1 nm·rad. 25% of the storage ring circumference is of free straight sections (i.e. 195 m) for insertion devices and the radiofrequency and injection systems.

The NSLS II storage ring [4, 5] consists of 30 DBA cells, with straight sections alternating in length between 5 m and 8 m, and each one is achromatic. Therefore, the lattice has a 15 super-periods structure. In a super-period there are 24 quadrupoles, four quadrupoles at ends of each DBA cell and four between the bending magnets. Regarding to the nonlinear lattice elements, there are five chromatic sextupoles between the dipoles, and four geometric sextupoles in each end of the DBA cell, i.e. there are 26 sextupoles per super-period. The quadru-

		Number of units	Length [m]	Bending angle [°]	
Dipoles		60	2.62	6	B 0.4 T
Quadrupoles	L	30	0.4	0	Maximum B' 21 T/m
	S	330	0.3	0	21 T/m
Sextupoles	L	30	0.30	0	Maximum B'' 500 T/m^2
	M	120	0.25	0	500 T/m^2
	S	240	0.20	0	500 T/m^2

Table 2.1.1. Generic parameters for magnets of the NSLS II storage ring.

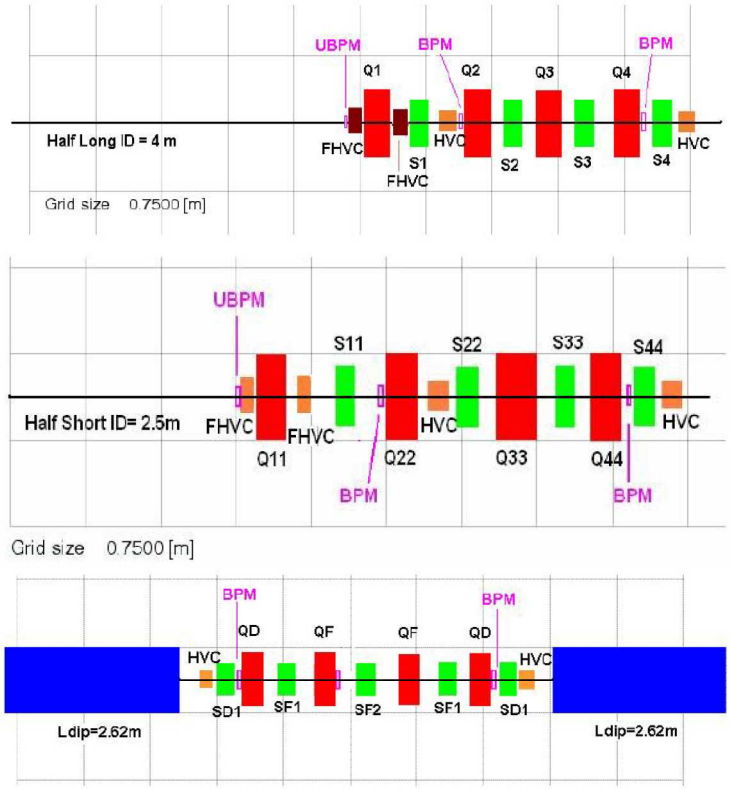

Figure 2.1.1. Layout for DBA cell of the NSLS II storage ring, in parts, up: part adjacent to long straight section, in middle: part adjacent to short straight section, down: between the two dipole magnets.

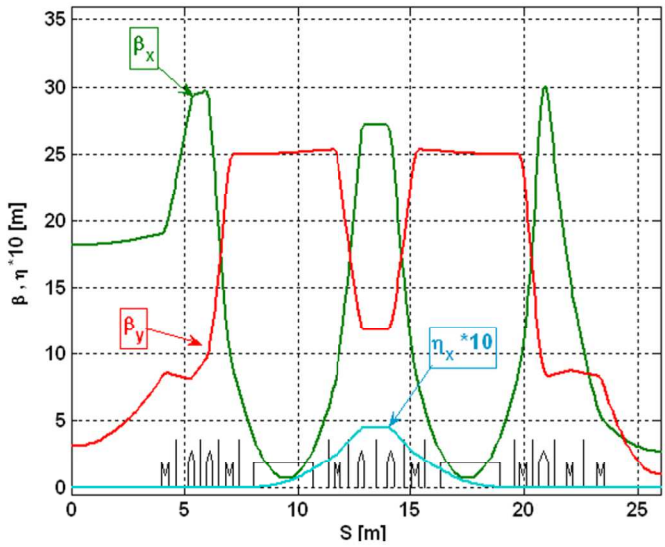

Figure 2.1.2. *Optical functions for AC10 operation mode of the SIRIUS storage ring. In this mode the optical functions are 10-fold symmetric.*

poles and sextupoles are individually powered but the current lattice design assumes 10 families (QD, QF, Q1, ..., Q4, Q11, ..., Q44) and 11 families (SD1, SF1, SF2, S1, ..., S4, S11, ..., S44), respectively. There are two type of dipoles that differ only by aperture size. Fig. 2.1.1 shows the details of DBA cell of the NSLS II storage ring, whereas in Table 2.1.1 are given some parameters of the magnets.

Fig. 2.1.2 shows the optical functions for the NSLS II storage ring whose working point is at the tunes $\nu_x = 32.35$ and $\nu_y = 16.28$. For bare lattice (i.e. without other nonlinear elements more than the sextupoles) the horizontal and vertical natural chromaticities are $\xi_x = -110$ and $\xi_y = -41.8$. As a consequence of lattice design, based on the classic DBA cell, the dynamic aperture is very robust, as demonstrated by the beam dynamics simulations [4].

2.2 Sirius

Currently, the SIRIUS 3rd generation light source is in planning (Brazil). Based on a novel lattice design, which involves high-field permanent dipoles, the SIRIUS storage ring will have a horizontal emittance of 0.28 nm·rad, 3 GeV of energy and 500 mA of current (in multibunch operation mode). The circumference length is 518 m, of which 130 m (i.e. 25%) are available for straight sections.

The SIRIUS storage ring [6, 7] is composed of 20-cells 5-bend achromat (5BA), Fig. 2.2.1 shows a schematic of one of these cells. Each achromat is separated by straight sections of 7 m and 6 m in alternate way. There are four dipole families, B1, B2, B3 and BC, the thin permanent dipoles (BC) of 2 T are sandwiched in the center of two dipoles B3, B3-BC-B3, in order to produce a longitudinal field gradient, which helps reduce the emittance and also creates a hard x-ray dipole source (12 keV critical energy) with modest total energy loss. Further, the SIRIUS lattice have ten quadrupole families (QAF, QAD, QBF, QBD1, QBD2, QF1, ..., QF4) and nine sextupole families (SA1, SA2, SB1, SB2, SF1, SF2, SD1, SD2, SD3). A summary of main parameters of the magnets are given in Tables 2.2.1-2.2.3.

The quadrupole QBD2 plays a special role, because the 7 m straight sections are exactly the same as the 6 m ones except by said quadrupole. When this quadrupole is zeroed the two straight sections are identical from the optics point of view. Such that the SIRIUS storage ring has two operation modes, one with

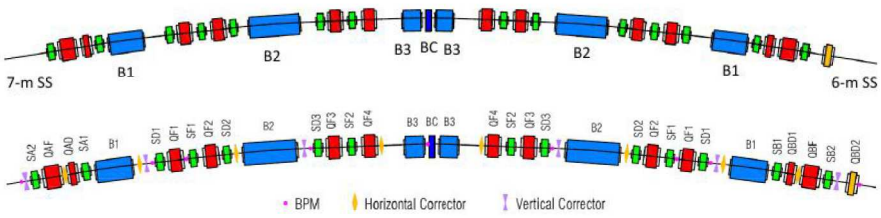

Figura 2.2.1. Layout for the 5BA cell of SIRIUS storage ring. Dipoles, quadrupoles and sextupoles are indicated in blue, red and green, respectively. The 6 m straight section is exactly the same as the 7 m one except for an extra quadrupole at the extremity (picture below), shown in orange at the right side.

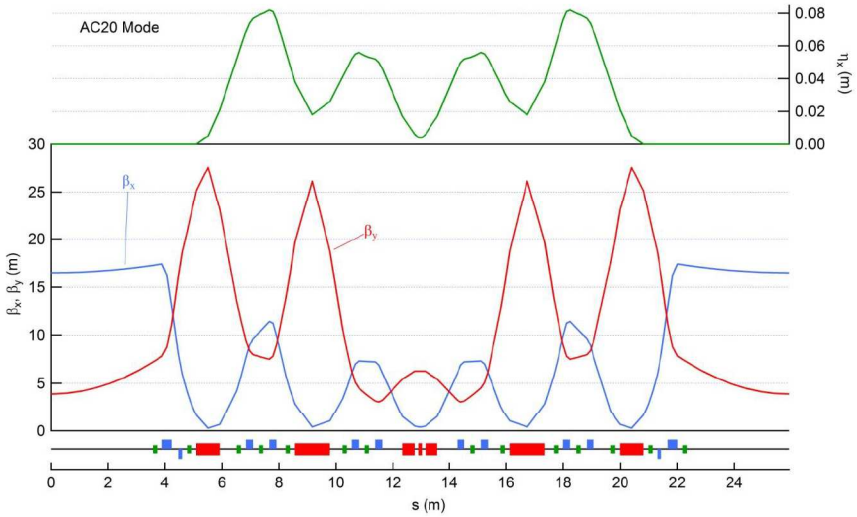

Figure 2.2.2. Optical functions for AC20 operation mode of the SIRIUS storage ring. In this mode the optical functions are 20-fold symmetric.

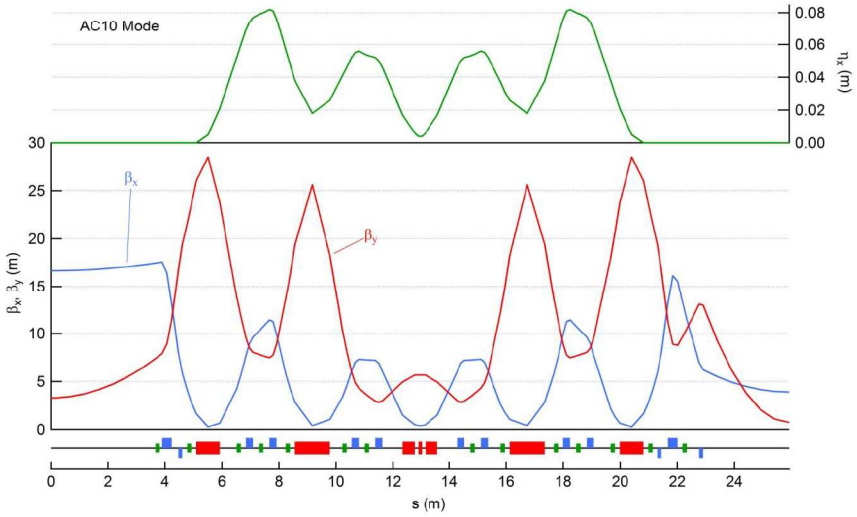

Figure 2.2.3. Optical functions for AC10 operation mode of the SIRIUS storage ring. In this mode the optical functions are 10-fold symmetric.

Dipole	B1	B2	B3	BC	Units
Number of units	40	40	40	20	–
Length	0.828	1.228	0.428	0.125	m
Bending angle	2.77	4.10	1.43	1.4	°
Bending radius	17.150	17.150	17.150	5.131	m
Dipole field (B)	0.584	0.584	0.584	1.95	T
Gradient field (B')	−7.8	−7.8	−7.8	0	T/m

Table 2.2.1. Parameters of bending magnets of the SIRIUS storage ring.

Quadrupole	QF	QD	QFC	Units
Number of units	40	60	160	–
Length	0.34	0.14	0.25	m
Maximum quadrupole field ($\|B'\|$)	40	40	40	T/m
Maximum strength ($\|B'/B\rho\|$)	4	4	4	m^{-2}

Table 2.2.2. Parameters of SIRIUS quadrupole magnets. The notation is as follows: QD={QAD, QBD1, QBD2}, QF={QAF, QBF} and QFC={QF1, ... QF4}.

Sextupole	Generic	Units
Number of units	280	–
Length	0.15	m
Maximum sextupole field ($\frac{1}{2}\|B''\|$)	2335	T/m^2
Maximum integrated strength ($\frac{1}{2}\|B''L/B\rho\|$)	35	m^{-2}

Table 2.2.3. Generic parameters of sextupole families of the SIRIUS storage ring.

10-fold symmetry (named AC10) when QBD2 is on, and other with 20-fold symmetry (named AC20) when QBD2 is off.

Optical functions for both operation modes (AC20 and AC10) of the SIRIUS storage ring are shown in Figs. 2.2.2 and 2.2.3. Certainly, the working point of the AC20 operation mode, at tunes $\nu_x = 44.60$ and $\nu_y = 11.64$, is different to working point of the AC10 operation mode, at tunes $\nu_x = 46.25$ and $\nu_y = 14.15$. The same happens with the natural chromaticities for the bare lattice, i.e. error free, namely, $\xi_x = -108.0$ and $\xi_y = -72.8$ for AC20 mode, and $\xi_x = -113.2$ and $\xi_y = -80.1$ for AC10 mode. Simulations show that the dynamic aperture is better in the higher symmetry mode (AC20).

2.3 Max IV

MAX IV is the next step for the development of MAX-lab (Sweden), and it is currently under construction. The new laboratory will have two storage rings [8] and the design also includes an option for a Free Electron Laser as a second development stage of the facility. A storage ring will have electron energy of 1.5 GeV and a circumference of 96 m, and the other will have electron energy of 3 GeV and a circumference of 528 m. Only the bigger ring is interesting for the present work.

The MAX IV 3 GeV storage ring (or simply MAX IV storage ring) has been designed using a novel multibend achromat lattice, with magnets very compact including several combined functions, so that the horizontal emittance will be around 0.326 nm·rad. In multibunch operation mode the electron beam nominal current is of 500 mA.

The MAX IV storage ring is composed of 20-cells 7-bend achromat (7BA) which are separated by long straight sections (LongStr) of 4.8 m, each achromat consists of five unit cells plus two matching cells, see Fig. 2.3.1. As show in Fig. 2.3.1, the matching cells are separated from matching cells by short straight sections (ShortStr) of 1.3 m; thus, 28% of the storage ring is of straight sections, namely 148 m. There are three families of combined dipoles with vertical focu-

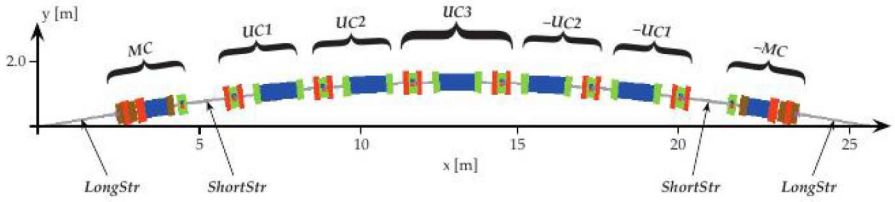

Figura 2.3.1. Layout for a 7BA achromat cell of the MAX IV storage ring.

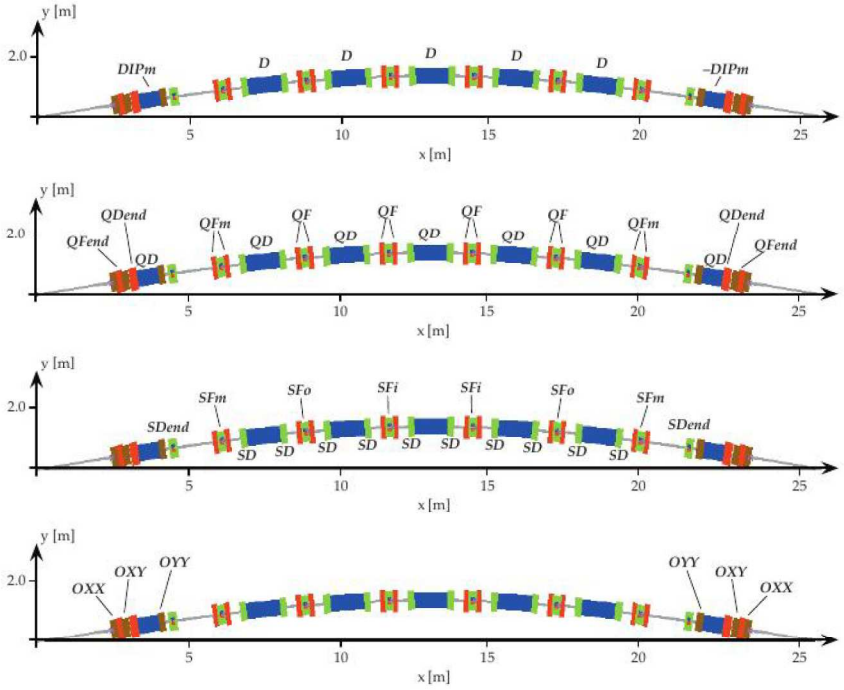

Figure 2.3.2 Magnets distribution in the 7BA cell of the MAX IV storage ring, from top to bottom: dipoles, quadrupoles, sextupoles and octupoles.

sing gradient (QD): D, DIPm and −DIPm; note that −DIPm is obtained from DIPm by inverting its components along the s coordinate. This gradient field QD almost removes the need for dedicated defocusing quadrupoles making the lattice more compact and at the same time allows for a decrease in horizontal emittance. Additionally, the cell contains four quadrupole families (QF, QFm, QFend and QDend), five sextupole families (SD, SDend, SFm, SFo, SFi) and three octupole families (OXX, OXY and OYY), its distribution along the 7BA cell is shown in Fig. 2.3.2. Dipoles have a complex structure, so that for the beam dynamics simulations these have been modeled with several dipole magnet slices,

$$\begin{aligned} D &= (DIP, -DIP) \\ DIP &= (Df5, Df4, Df3, Df2, Df1, D0) \\ DIPm &= (Ds6, Ds5, Ds4, Ds3, Ds2, Ds1, Ds0, \\ &\quad Dm1, Dm2, Dm3, Dm4, Dm5)\,. \end{aligned}$$

Family	D	DIPm	−DIPm
Number of units	100	20	20
Length	1.224 m	0.754 m	0.754 m
Bending angle	3°	1.5°	1.5°
Bending radius	23.372 m	28.810 m	28.810 m
Maximun dipole field (B)	0.528 T	0.532 T	0.532 T
Maximun gradient field (B')	−8.667 T/m	−8.725 T/m	−8.725 T/m

Table 2.3.1. Main parameters of combined bending magnets of the MAX IV storage ring.

Magnet slice	Bending angle [°]	Dipole field B [T]	Gradient field B' [T/m]	Length [m]
Df5	0.00009	0.0003	−0.0013	0.0500
Df4	0.00157	0.0055	0.1177	0.0500
Df3	0.10186	0.3558	−5.5221	0.0500
Df2	0.15110	0.5278	−8.6666	0.0500
Df1	0.15120	0.5281	−8.6551	0.0500
D0	1.09418	0.5281	−8.6546	0.3619
Ds6	0.00107	0.0037	0.0661	0.0500
Ds5	0.05073	0.1772	−2.7162	0.0500
Ds4	0.07467	0.2608	−4.2541	0.0500
Ds3	0.07625	0.2663	−4.2634	0.0500
Ds2	0.11498	0.4016	−5.8529	0.0500
Ds1	0.15205	0.5311	−8.7095	0.0500
Ds0	0.62170	0.5316	−8.7130	0.2042
Dm1	0.15222	0.5317	−8.7135	0.0500
Dm2	0.15212	0.5314	−8.7251	0.0500
Dm3	0.10255	0.3582	−5.5594	0.0500
Dm4	0.00158	0.0055	0.1185	0.0500
Dm5	0.00009	0.0003	−0.0013	0.0500

Table 2.3.2. Parameters for the slices used to model the bending magnets in the MAX IV storage ring.

The slices have different dipole strengths to model the longitudinally varying field strengths. Main parameters of MAX IV magnets are given in Tables 2.3.1-2.3.5.

Some of most important features of the focussing system are that the QFm family is most efficient to adjust the dispersion in the straight sections, and to move the tunes adequately a small variation of the field strengths of QD and QF families should be sufficient. The families QFend and QDend are introduced for matching in the straight sections. With this focussing system, the linear optics of the MAX IV storage ring have been tuned in such a way to achieve a working point at tunes $\nu_x = 42.20$ and $\nu_y = 14.28$. Fig. 2.3.3 shows the beta and dispersion functions for a 7BA achromat, while Fig. 2.3.4 shows the machine working point. In order to correct the large natural negative chromaticity,

$$\begin{aligned} \xi_x^{\mathrm{n}} &= -49.8\,, \\ \xi_y^{\mathrm{n}} &= -43.9\,, \end{aligned}$$

Family	Slice	Number of units	Length [m]	Strength [m^{-2}] $b_2 = \frac{B'}{B\rho}$	Quadrupole field B' [T/m]
QF	–	160	0.1500	4.0301	40.329
QFm	–	80	0.1500	3.7740	37.766
QFend	–	40	0.2500	3.6538	36.564
QDend	–	40	0.2500	−2.5037	−25.054
QDIP	QDf5	200	0.05000	−0.0001	−0.0013
	QDf4	200	0.05000	0.0118	0.1177
	QDf3	200	0.05000	−0.5518	−5.5221
	QDf2	200	0.05000	−0.8661	−8.6666
	QDf1	200	0.05000	−0.8649	−8.6551
	QD0	200	0.36189	−0.8649	−8.6546
QDIPm	QDs6	40	0.05000	0.0066	0.0661
	QDs5	40	0.05000	−0.2714	−2.7162
	QDs4	40	0.05000	−0.4251	−4.2541
	QDs3	40	0.05000	−0.4260	−4.2634
	QDs2	40	0.05000	−0.5849	−5.8529
	QDs1	40	0.05000	−0.8704	−8.7095
	QDs0	40	0.20424	−0.8707	−8.7130
	QDm1	40	0.05000	−0.8708	−8.7135
	QDm2	40	0.05000	−0.8719	−8.7251
	QDm3	40	0.05000	−0.5556	−5.5594
	QDm4	40	0.05000	0.0118	0.1185
	QDm5	40	0.05000	−0.0001	−0.0013

Table 2.3.3. Parameters for the four quadrupole families of the MAX IV storage ring, the quadrupole field integrated to dipoles is also included.

Family	Number of units	Length [m]	Strength [m^{-3}] $b_3 = \frac{1}{2}\frac{B''}{B\rho}$	$b_3 L$ [m^{-2}]	Sextupole field B'' [T/m^2]
SD	200	0.1	−116.63	−11.663	−2334.1
SDend	40	0.1	−170.00	−17.000	−3402.4
SFm	40	0.1	170.00	17.000	3402.4
SFo	40	0.1	174.00	17.400	3482.4
SFi	40	0.1	207.41	20.741	4151.1

Table 2.3.4. Main parameters for the five sextupole families of the MAX IV 7BA lattice.

Family	OXX	OXY	OYY
Number of units	40	40	40
Length	0.1 m	0.1 m	0.1 m
Octupole field (m_4)	−13144 T/m^3	21816 T/m^3	−6886 T/m^3

Table 2.3.5. Main parameters for the three octupole families of the MAX IV storage ring.

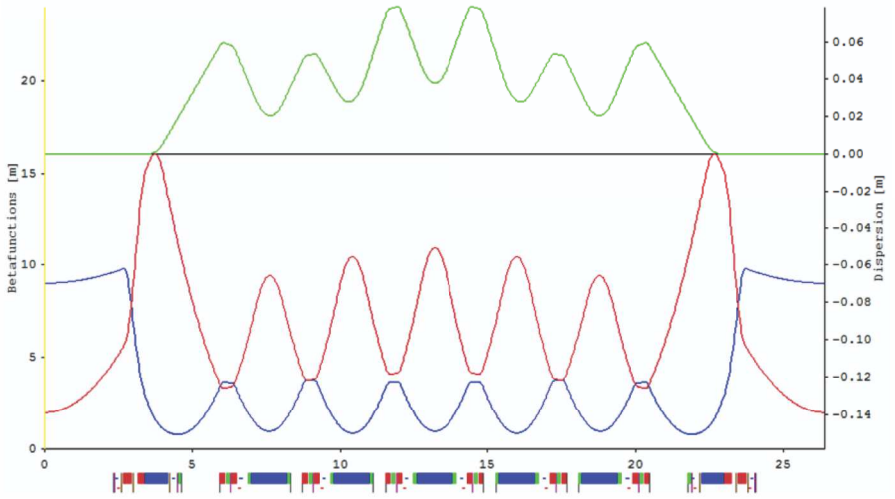

Figure 2.3.3. Lattice functions for the MAX IV 3 GeV storage ring, the horizontal and vertical beta functions are shown in blue and red, respectively, while the horizontal dispersion is shown in green.

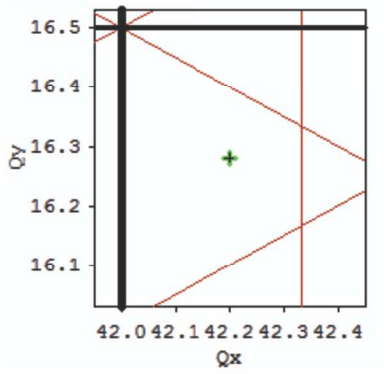

Figure 2.3.4. Working point of the MAX IV 3 GeV storage ring bare lattice, resonance lines have been included up to third order.

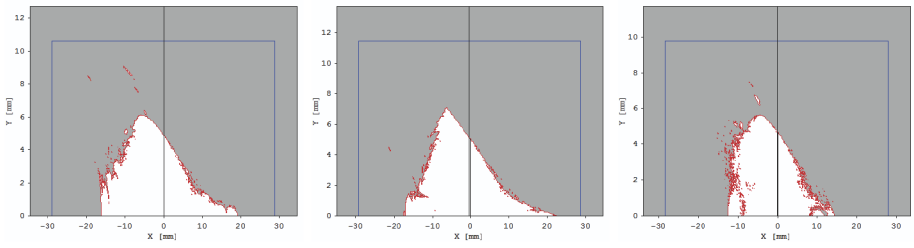

Figure 2.3.5. Dynamic aperture at the start ($s = 0$) of the MAX IV 3 GeV storage ring bare lattice. The tracking was performed with OPA in 2D. From left to right: for on-momentum particles $\delta p/p = 0.0\%$, and for off-momentum particles $\delta p/p = 2.0\%$ and $\delta p/p = -2.0\%$.

two families of strong sextupoles are required. The families designated to correct the natural chromaticities are SD and SFi, because they are located where the dispersion is higher and therefore they are more efficient. After correction, the chromaticity values are small and positive,

$$\xi_x^c = 1.0\,, \tag{1}$$

$$\xi_y^c = 1.0\,. \tag{2}$$

Additional sextupoles are necessary to reduce the undesirable nonlinear effects introduced by the sextupoles that compensate the natural chromaticities, besides to nonlinear effects that are inherent to any physical lattice, for example, those due to magnet fringe fields, magnet imperfections, misalignments, etc. Because the MAX IV sextupoles are very strong, their second-order effects can reduce the dynamic aperture (DA) significantly, octupole magnets are the obvious solution to this new problem. The nonlinear lattice of MAX IV storage ring (sextupoles and octupoles) ensures that the DA is sufficient to achieve the required beam lifetime and increase injection efficiency. Fig. 2.3.5 shows the DA for the storage ring without octupoles, of course, this is not the actual DA of the lattice, however, this will be useful as reference in this study.

2.4 ESRF upgrade phase II

The European Synchrotron Radiation Facility (ESRF), located in France, has a storage ring of 844 m circumference with a 32-cell double-bend achromat (DBA) lattice and an energy of 6 GeV [9]. In multibunch operation mode the electron beam has a nominal current of 200 mA, and the horizontal emittance is 4 nm·rad. Fig. 2.4.1 shows a DBA cell and the optical functions. The 32 DBA cells are arranged in 16 super-period cells; all DBA cells have the same magnets and each is separated by a straight section of 6 m long, where insertion devices (ID) of up to 5 m long can be installed. Altogether, the storage ring consists of 64 bending magnets, 320 quadrupoles and 224 sextupoles, while 23% of it is straight sections (i.e. 192 m).

Currently, ESRF is undergoing the first phase of an upgrade program [10], in which some storage ring straight sections have been lengthened, of course, by modifying some DBA cells. Therefore, some data given in the previous paragraph may be incorrect today. Phase II of this program involves change the storage ring lattice [11, 12], from DBA-cell structure to a 7DB-cell structure.

The new lattice of ESRF storage ring is composed of 32 cells 7BA, each 7BA cell is composed of 31 magnets, which are shown in Fig. 2.4.2 where the optical functions are also shown. The seven dipoles of each cell consist of three short magnets (central part) with 0.34 T and 0.86 T, according to values requested by the beamlines, and with strong transverse gradients, from 45 T/m to 50 T/m. The four remaining dipoles (ends) include a longitudinally varying field ranging typically from 0.6 T to 0.15 T, dipole structure is segmented into 5 similar modules with different amounts of permanent magnet volumes to achieve this longitudinal field. High-gradient quadrupoles and sextupoles are need, but the magnet technology imposes constraints on the quadrupole and sextupole strengths which must be less than 100 T/m and 1500 T/m^2, respectively.

This storage ring lattice is able to reduce the horizontal emittance to 150 pm·rad. The tunes ($\nu_x = 75.580$ and $\nu_z = 27.620$) and natural chromaticities ($\xi_x = -96$ and $\xi_z = -72$) also differ from their original values. However, the e-

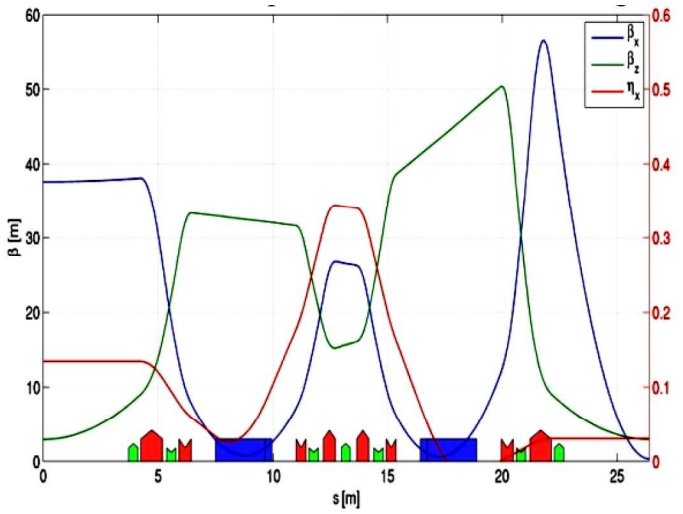

Figura 2.4.1. Lattice functions and layout for a DBA cell of the current ESRF storage ring. At bottom the dipoles, quadrupoles and sextupoles are shown in blue, red and green, respectively.

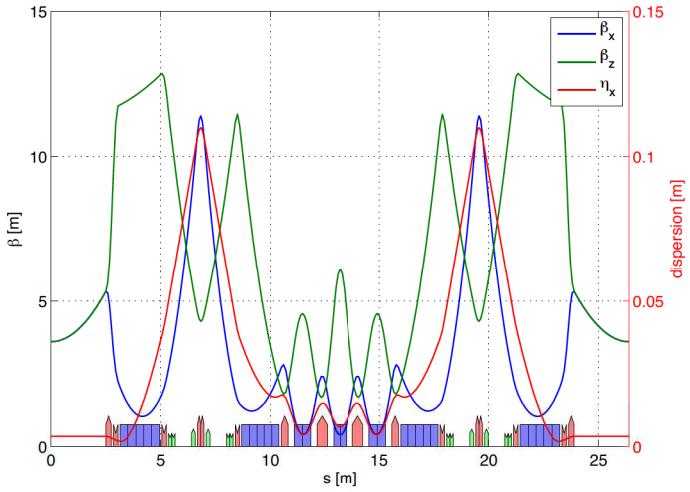

Figura 2.4.2. Lattice functions and layout for the new 7BA cell of ESRF storage ring.

nergy (6 GeV), circumference lenght (844 m) and current (200 mA) of storage ring are kept. Further, the beamline source points remain unchanged, both the ID source points and the existing bending-magnet beamlines.

2.5 Diamond upgrade

The DIAMOND 3rd generation light source, located in the UK, has a storage ring of 561.6 m circumference and operates at an energy of 3 GeV [13, 14]. 24 DBA cells compose the whole lattice, which has 6 fold structure and has been

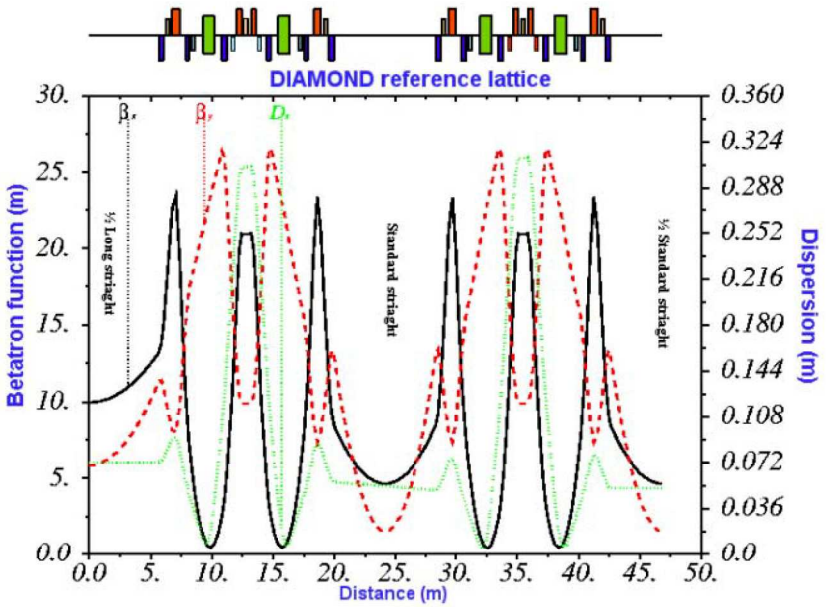

Figure 2.5.1. Optics functions for $1/12^{\text{th}}$ of the DIAMOND storage ring. At top the magnets (dipoles, quadrupoles and sextupoles) and straight sections (LS and SS) are indicated.

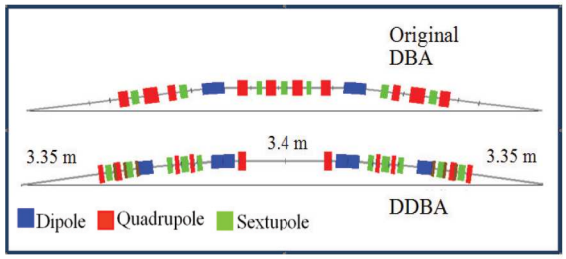

Figura 2.5.2. Layout of the DBA cell (top) of the current storage ring and layout of the modified DDBA cell (bottom) for lattice upgrade.

optimized to generate an electron beam of high brightness, the horizontal emittance is 2.75 nm·rad and the beam current is 300 mA. The *main structure* of the lattice is as follow: ($\frac{1}{2}$-LS, DBA, SS, DBA, SS, DBA, SS, DBA, $\frac{1}{2}$-LS), where LS and SS are the long straight section of 8 m and standard straight section of 5 m, respectively, the ends DBA-cells and middle DBA-cells has magnets with different settings. Fig. 2.5.1 shows the optical functions for half of such *main structure*, the layout of the lattice is also shown at the top. Note that only 25% of the circumference (i.e. 138 m) is available for straight sections.

At DIAMOND the main goal of the upgrade studies [15, 16] is not to reduce the emittance, as in most studies of this type, but to introduce additional insertion devices and hence increase the capacity of the facility. The scheme involves converting some of the original DBA cells into a double-DBA (DDBA), with a new straight section of 3.4 m between the two achromats. This new cell is shown in Fig. 2.5.2, where the existing DBA cell is also shown, the optical functions are displayed in Fig. 2.5.3.

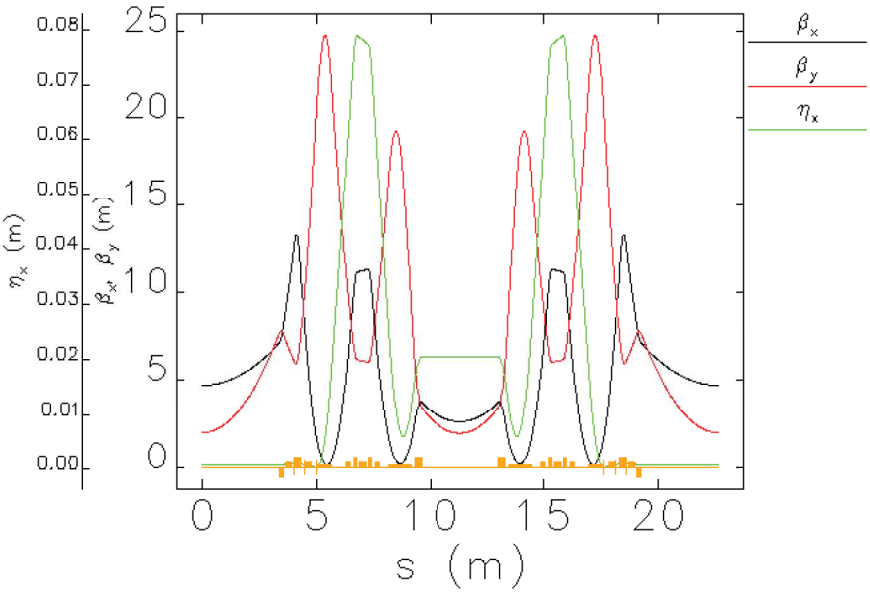

Figure 2.5.3. Optics functions of the modified DDBA cell.

DDBA cell consists of four dipoles, ten quadrupoles and ten sextupoles, 24 magnets, twenty-four magnets in total (original DBA cell has nineteen magnets). To control the optics functions in the DDBA cell, a strong focusing is required, which is achieved by introducing a horizontal defocusing quadrupole gradient in the dipole and strong quadrupoles in the cell. Beam dynamics simulations show that the quadrupole gradients required reach 70 T/m and the quadrupole gradient in the dipole is 14 T/m while the dipole field is 0.8 T. Sextupoles are limited to a gradient of 4000 T/m^2.

With two DDBA cells, installed between two standard straight sections asymmetrically in the DIAMOND lattice, the new horizontal emittance is 2.50 nm·rad. The length of the storage ring that is available to straight sections has a modest increase to 144.8 m, which now accounts for 26%.

2.6 Soleil

SOLEIL is the French third generation light source [17, 18], it has a emittance electron beam of 3.91 nm·rad and a maximum current of 430 mA in the multi-bunch mode. The storage ring operates to an energy of 2.75 GeV, and its circumference is of 354 m. DBA cells and straight sections compose the lattice, at the bottom of Fig. 2.6.1 one-eighth of the whole lattice is shown. In which, the layout is as follow (from left): a long straight section (SDL), a DBA matching cell, a medium straight section (SDM), a DBA unit cell, which has a short straight section (SDC) in between, and a SDM. As usual, the DBA cells are comprised of two dipoles, quadrupoles and sextupoles. Magnet's parameters are irrelevant for present purposes, only the number of dipoles (32) and DBA cells (16) are important. However, the straight section lengths are relevant, these are

$$L(\mathrm{SDL}) \quad = \quad 12\,\mathrm{m}\,,$$

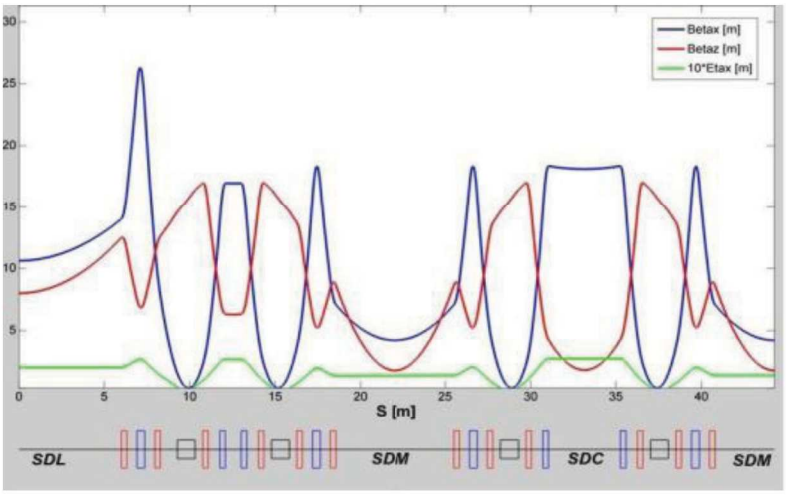

Figure 2.6.1. Optics functions for $1/8^{\text{th}}$ of the SOLEIL storage ring. Positions of the magnets (dipoles, quadrupoles and sextupoles) and straight sections (SDL, SDM and SDC) are indicated at the bottom.

$$\begin{aligned} L(\text{SDM}) &= 7\,\text{m}\,, \\ L(\text{SDC}) &= 3.6\,\text{m}\,. \end{aligned}$$

Thus, 45% of the storage ring circumference is of straight sections, that is, 160.8 m. These are used for the injection and radio-frequency systems, and to deliver photons to 26 beamlines.

Fig. 2.6.1 shows the optical functions for the SOLEIL storage ring, the horizontal dispersion function, η_x, and the horizontal and vertical beta functions, β_x and β_z, respectively.

2.7 Alba

ALBA is a 3 GeV synchrotron light source, the storage ring has a circumference of 268.8 m and has been designed for a maximum current of 400 mA. The lattice is based on a DBA structure, has four fold symmetry and provides low emittance of the beam, the nominal value is 4.4 nm·rad [19, 20]. It is known that such lattices, with low emittance, require strong sextupole magnets to compensate natural chromaticities while their arrangement should increase the dynamic aperture. In this regard, it is noteworthy that the ALBA dynamic aperture optimization is very well made.

The lattice of ALBA storage ring has one family of dipoles (D) with gradient field (QD), three families of defocusing quadrupoles (QD1, ...) and eight families of focusing quadrupoles (QF1, ...), five families of defocusing sextupoles (SD1, ...) and four families of focusing sextupoles (SF1, ...). In Fig. 2.7.1, the optical functions of an *arc* for the nominal lattice are shown, said arc consists of four DBA cells, two matching cells in the ends and two unit cells in the medium. Within the arc, drift spaces separate the DBA cells, which are called medium s-

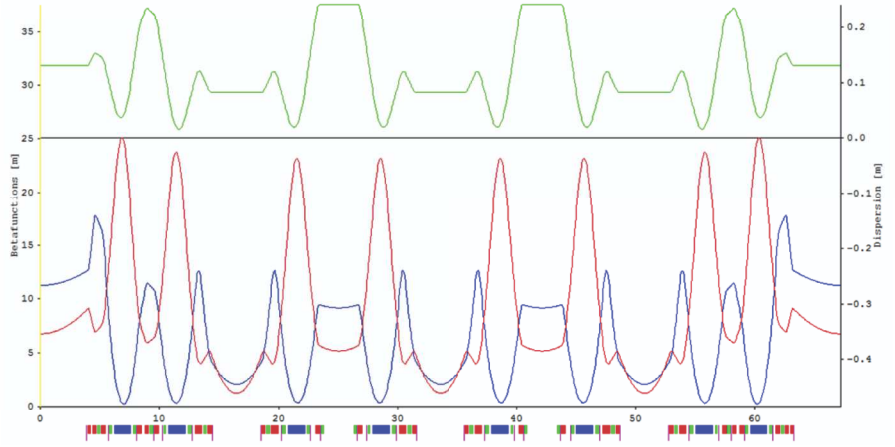

Figure 2.7.1 Optics functions for an arc of the ALBA storage ring as calculated by OPA; the beta functions β_x and β_y, and the horizontal dispersion D_x are shown in blue, red and green, respectively. The positions of the dipoles (blue), quadrupoles (red) and sextupoles (green) are indicated at the bottom.

Number of units	32
Length	1.374 m
Bending angle	11.25°
Bending radius	6.997 m
Dipole field (B)	1.430 T
Gradient field (B')	−5.673 T/m

Table 2.7.1. Main parameters for the bending magnets of the ALBA storage ring.

Family	Number of units	Length [m]	Strength [m^{-2}] $b_2 = \frac{B'}{B\rho}$	Quadrupole field B' [T/m]
Integrated to dipole	32	1.3739	−0.5669	−5.673
QD1	8	0.2295	−1.7745	−17.757
QD2	8	0.2891	−1.9373	−19.386
QD3	16	0.2892	−1.9350	−19.364
QF1	8	0.2902	1.5714	15.725
QF2	8	0.2891	1.8467	18.480
QF3	8	0.2901	1.6412	16.423
QF4	8	0.2299	1.3997	14.006
QF5	8	0.3096	1.7973	17.986
QF6	8	0.5277	2.0906	20.921
QF7	16	0.5282	2.0544	20.559
QF8	16	0.3088	2.0063	20.077

Table 2.7.2. Parameters for the eleven quadrupole families of the ALBA storage ring, the quadrupole field integrated to dipole is also included.

Family	Number of units	Length [m]	Strength [m^{-3}] $b_3 = \frac{1}{2}\frac{B''}{B\rho}$	$b_3 L$ [m^{-2}]	Sextupole field B'' [T/m^2]
SD1	8	0.1709	−23.10	−3.947	−462.3
SD2	8	0.1704	−20.90	−3.561	−418.2
SD3	8	0.1700	−26.53	−4.510	−531.0
SD4	24	0.2408	−25.77	−6.205	−515.8
SD5	16	0.1699	−31.09	−5.282	−622.2
SF1	8	0.1730	12.90	2.231	258.2
SF2	8	0.2408	23.41	5.636	468.5
SF3	24	0.2407	26.38	6.349	527.9
SF4	16	0.1718	19.09	3.280	382.1

Table 2.7.3. Parameters for the nine sextupole families of the ALBA storage ring.

traight sections (MSS) and have a length of 4.0 m, so that there are three MMS in each arc. The magnets arrangement in the matching cell is as follow

$$(\mathrm{QD1}, \mathrm{QF1}, \mathrm{SF1}, \mathrm{QF2}, \mathrm{SD1}, \mathrm{D}, \mathrm{SD2}, \mathrm{QF3}, \mathrm{QF4},$$
$$\mathrm{SF2}, \mathrm{QF5}, \mathrm{SD3}, \mathrm{D}, \mathrm{SD4}, \mathrm{QF6}, \mathrm{SF3}, \mathrm{QD2})\,,$$

while in the unit cell the arrangement is

$$(\mathrm{QD3}, \mathrm{SF3}, \mathrm{QF7}, \mathrm{SD4}, \mathrm{D}, \mathrm{SD5}, \mathrm{QF8}, \mathrm{SF4},$$
$$\mathrm{SSS}, \mathrm{SF4}, \mathrm{QF8}, \mathrm{SD5}, \mathrm{D}, \mathrm{SD4}, \mathrm{QF7}, \mathrm{SF3}, \mathrm{QD3})\,,$$

SSS denotes a short straight section of 2.3 m. In Figure 2.7.1, the magnets posions are also shown. Four arcs make up the whole ALBA storage ring, which are separated by drift spaces having a length of 7.8 m each, and are called long straight sections (LSS).

Main parameters of the magnets are given in Tables 2.7.1-2.7.3, were also included parameters that are very useful for the simulation programs, as the quadrupole and sextupole strengths (b_2 and b_3, respectively), and the integrated sextupole strength ($b_3 L$). With these settings the working point of ALBA storage ring bare lattice is located at tunes $\nu_x = 18.155$ and $\nu_y = 8.362$, see Fig. 2.7.2. And the dynamic aperture which is achieved for on- and off-momentum particles is shown in Fig. 2.7.3. For the bare lattice, the horizontal and vertical natural chromaticity compensated by the sextupoles are

$$\begin{aligned} \xi_x^{\mathrm{n}} &= -40.18\,, \\ \xi_y^{\mathrm{n}} &= -27.05\,, \end{aligned}$$

and then the corrected chromaticities are

$$\begin{aligned} \xi_x^{\mathrm{c}} &= 1.62\,, \\ \xi_y^{\mathrm{c}} &= 4.59\,. \end{aligned}$$

Other fundamental components of a synchrotron are straight sections, ALBA storage ring has four LSS, twelve MSS and eight SSS, altogether it has 97.6 m of free straight sections, this is the 36% of circumference. Insertion Devices for experiments are installed in the MSS, while the radio frequency and injection systems are installed is the LSS.

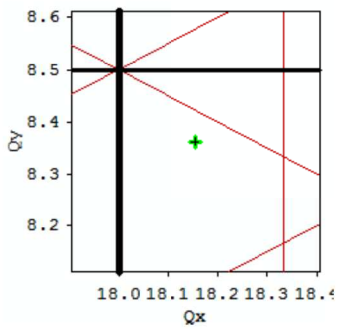

Figure 2.7.2. Working point of the ALBA storage ring bare lattice, resonance lines have been included up to third order.

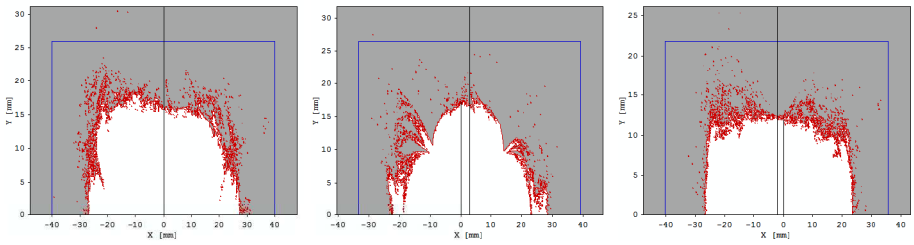

Figure 2.7.2. Dynamic aperture at the start ($s = 0$) of ALBA storage ring bare lattice. The tracking was performed with OPA in 2D. From left to right: for on-momentum particles $\delta p/p = 0.0\%$, and for off-momentum particles $\delta p/p = 2.0\%$ and $\delta p/p = -2.0\%$.

3 Linear Lattice Designs

In this section I present four storage ring lattices that can be the starting point of the Mexican project, at the request of the project leader[1], the conceptual designs should preferably have a lower emittance to 2 nm·rad. As mentioned above, these designs are based on MAX IV and ALBA lattices, which are described in Sec. 2.3 and 2.7, respectively. All new lattices have the energy fixed in 3 GeV, as the original designs. Using the ALBA design two new lattices were created, one with 20 DBA cells that produce a storage ring of 336 m length, and other with 24 DBA cells and 403.2 m length for the resulting storage ring. The DBA cells are arranged in structures called arcs, see Sec. 2.7, so that the 20-cells storage ring has a structure of 5 arcs, while the one of 24 cells has 6 arcs. The same number of new lattices were created with the MAX IV design, one with thirteen 7BA cells and other with fifteen 7BA cells, the lengths of the resulting storage rings are 343.2 m and 396 m, respectively. So there are two pairs of lattices, each with similar lengths of the storage rings but different magnetic structures. In the Table 3.1 is given a summary of the most important features of the new lattices, further includes a label whose sole purpose is streamline the discussion.

[1]Matías Moreno Yntriago, Instituto de Física, Universidad Nacional Autónoma de México, e-mail: matias@fisica.unam.mx.

Label	M15-MX	M13-MX	A24-MX	A20-MX
Magnetic lattice structure	MAX-IV 7BA	MAX-IV 7BA	ALBA DBA	ALBA DBA
Number of cells	15	13	24	20
N-fold symmetry	15	13	6	5
Circumference [m]	396	343.2	403.2	336
Percentage of straight sections [%]	28	28	36	36
Horizontal emittance [nm·rad]	0.78	1.19	1.3	2.3

Table 3.1. Some general features for magnetic structure of the new storage rings, including a label for each lattice version.

Version	Number of units	Bending angle [°]	Dipole field B [T]	Length [m]
A24-MX	48	7.5	0.953	1.374
A20-MX	40	9	1.144	1.374
Alba	32	11.25	1.430	1.374

Table 3.2. Main parameters of dipoles of the A24-MX and A20-MX storage ring, for reference, parameters of the original dipoles are also given.

Version	Dipole type	Number of units	Bending angle [°]	Maximun dipole field [T]	Length [m]
M13-MX	D	65	4.6154	0.8125	1.2238
	DIPm	13	2.3077	0.8180	0.7542
	−DIPm	13	2.3077	0.8180	0.7542
M15-MX	D	75	4	0.7042	1.2238
	DIPm	15	2	0.7090	0.7542
	−DIPm	15	2	0.7090	0.7542
Max IV	D	100	3	0.5281	1.2238
	DIPm	20	1.5	0.5317	0.7542
	−DIPm	20	1.5	0.5317	0.7542

Table 3.3. Main parameters of dipoles of the M13-MX and M15-MX storage ring, for reference, parameters of the MAX IV dipoles are also given.

Two features of the new lattices require special mention, the emittance and the percentage of free straight sections having the storage rings, see Table 3.1. Both for the storage rings with the larger circumferences, A24-MX and M15-MX, as for those with the smaller circumferences, A20-MX and M13-MX, those based on the MAX IV design have the smaller emittance, below the 2 nm·rad required. Even more, the M15-MX lattice has a emittance of the order of subnanometers, 0.78 nm·rad; the A20-MX lattice has the largest emittance, 2.3 nm·rad, which is slightly greater than the required value. However, the storage

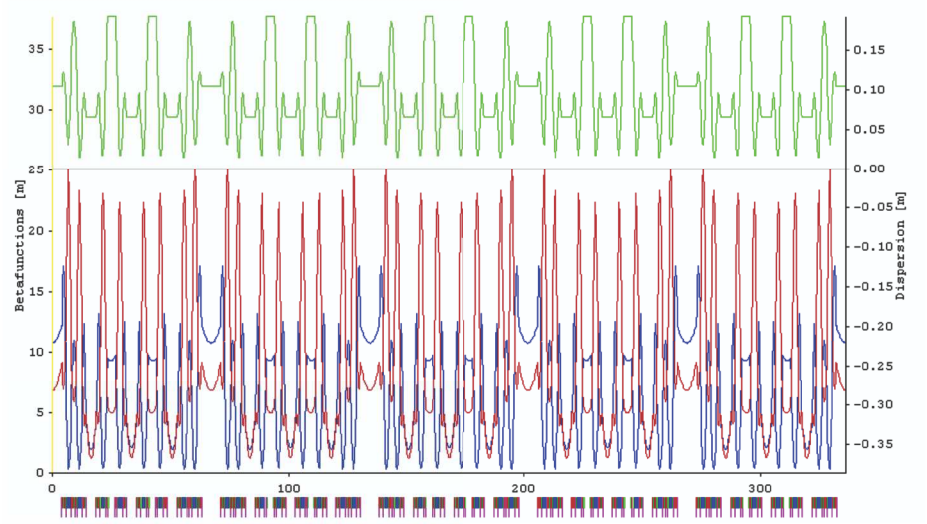

Figure 3.1 Optics functions of the whole A20-MX storage ring as calculated by OPA, the beta functions β_x and β_y, and the horizontal dispersion D_x are shown in blue, red and green, respectively. The positions of DBA cells are indicated at bottom.

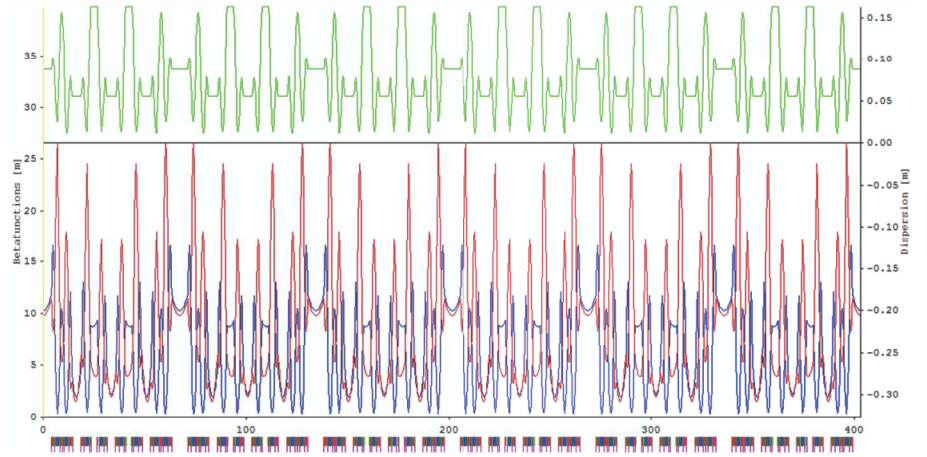

Figure 3.2 Optics functions for the whole A24-MX storage ring as calculated by OPA, the beta functions β_x and β_y, and the horizontal dispersion D_x are shown in blue, red and green, respectively. The positions of DBA cells are indicated at bottom.

rings based on the ALBA design provide a higher percentage of free straight sections (36% vs. 28% of the designs based on MAX IV).

In order to reduce the length of the MAX IV storage ring and increase the length of ALBA, the bending angles of the dipoles were modified as shown in Tables 3.2 and 3.3, for comparison purposes the original bending angles are also shown. In all cases the dipole lengths are kept equal to those of the original designs, in future studies this parameter can be modified. In these tables the number of dipoles and the magnetic dipole field is also given, the latter is important since for normal conducting magnets (steel) the maximum dipole fi-

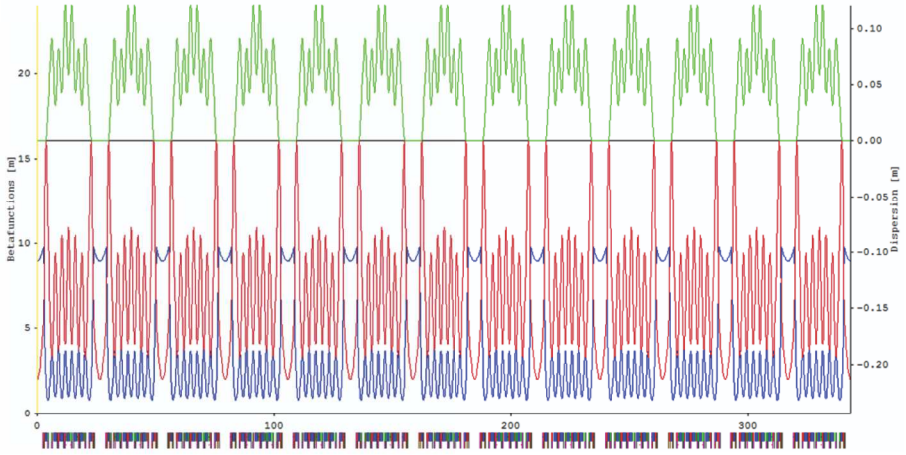

Figure 3.3. Optics functions of the whole M13-MX storage ring as calculated by OPA, the beta functions β_x and β_y, and the horizontal dispersion D_x are shown in blue, red and green, respectively. The positions of 7BA cells are indicated at bottom.

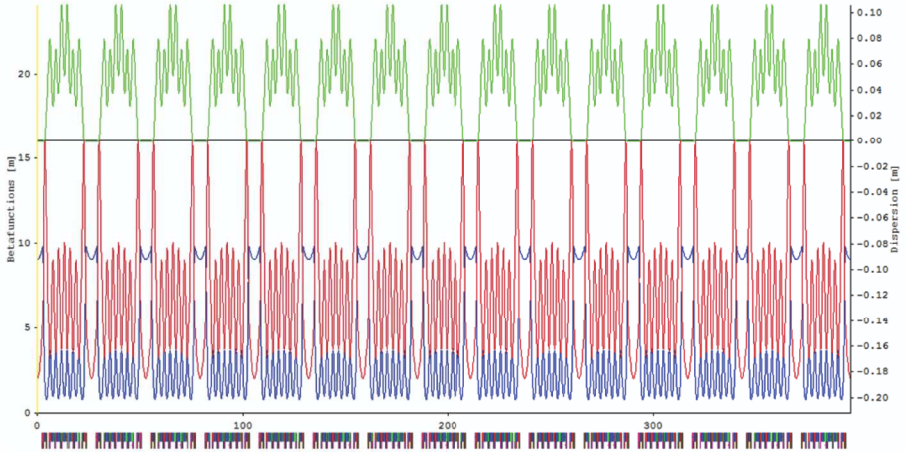

Figure 3.4. Optics functions for the whole M15-MX storage ring as calculated by OPA, the beta functions β_x and β_y, and the horizontal dispersion D_x are shown in blue, red and green, respectively. The positions of 7BA cells are indicated at bottom.

eld that can be obtained is 1.5 T [21], so all dipoles must be satisfy this constraint. Both the magnets based on ALBA design as the magnets based on MAX IV design have a gradient field, on which will be discussed below, however the MAX IV design has a more complex structure. In fact, these latter magnets are modeled with several dipole magnet slices, see Sec. 2.3.1 for more details. The parameters of such different slices in the M13-MX and M15-MX storage ring are shown in Table 3.4, of course, only the bending angles and the magnetic dipole fields are different with respect to original values, see Sec. 2.3.1, the lengths remain unchanged.

Version	Magnet slice	Bending angle [°]	Dipole field B [T]	Length [m]
M13-MX	Df5	0.0001	0.0005	0.0500
	Df4	0.0024	0.0084	0.0500
	Df3	0.1567	0.5474	0.0500
	Df2	0.2325	0.8120	0.0500
	Df1	0.2326	0.8125	0.0500
	D0	1.6834	0.8124	0.3619
	Ds6	0.0016	0.0058	0.0500
	Ds5	0.0780	0.2726	0.0500
	Ds4	0.1149	0.4013	0.0500
	Ds3	0.1173	0.4098	0.0500
	Ds2	0.1769	0.6179	0.0500
	Ds1	0.2339	0.8171	0.0500
	Ds0	0.9565	0.8179	0.2042
	Dm1	0.2342	0.8180	0.0500
	Dm2	0.2340	0.8175	0.0500
	Dm3	0.1578	0.5511	0.0500
	Dm4	0.0024	0.0085	0.0500
	Dm5	0.0001	0.0005	0.0500
M15-MX	Df5	0.0001	0.0004	0.0500
	Df4	0.0021	0.0073	0.0500
	Df3	0.1358	0.4744	0.0500
	Df2	0.2015	0.7037	0.0500
	Df1	0.2016	0.7042	0.0500
	D0	1.4589	0.7041	0.3619
	Ds6	0.0014	0.0050	0.0500
	Ds5	0.0676	0.2361	0.0500
	Ds4	0.0996	0.3478	0.0500
	Ds3	0.1017	0.3551	0.0500
	Ds2	0.1533	0.5355	0.0500
	Ds1	0.2027	0.7082	0.0500
	Ds0	0.8289	0.7088	0.2042
	Dm1	0.2030	0.7090	0.0500
	Dm2	0.2028	0.7085	0.0500
	Dm3	0.1367	0.4776	0.0500
	Dm4	0.0021	0.0074	0.0500
	Dm5	0.0001	0.0004	0.0500

Table 3.4. Main parameters for the slices used to model the bending magnets in the M13-MX and M15-MX storage ring.

Since the dipole strengths of the A20-MX and A24-MX storage rings are smaller than original strengths, these new lattices have a smaller dispersion than the ALBA lattice. In the case of the M13-MX and M15-MX storage rings the opposite happens, the dispersion increased with respect to the original lattice dispersion because the dipole strengths also increased. A consequence, as shown below, is that the sextupole strength configurations change in each case. Regarding the beta functions, it is preferable to try to reproduce their original values at each lattice point, especially in the straight sections, in order

Family	Number of units	Length [m]	Strength [m^{-2}] $b_2 = \frac{B'}{B\rho}$	Quadrupole field B' [T/m]
Integrated to dipole	40	1.3739	−0.5735	−5.739
QD1	10	0.2295	−1.7745	−17.757
QD2	10	0.2891	−1.9373	−19.386
QD3	20	0.2892	−1.9350	−19.364
QF1	10	0.2902	1.5714	15.725
QF2	10	0.2891	1.8467	18.480
QF3	10	0.2901	1.6412	16.423
QF4	10	0.2299	1.3997	14.006
QF5	10	0.3096	1.7973	17.986
QF6	10	0.5277	2.0906	20.921
QF7	20	0.5282	2.0544	20.559
QF8	20	0.3088	2.0063	20.077

Table 3.5. Main parameters for the eleven quadrupole families of the A20-MX storage ring, the quadrupole field integrated to dipole is also included.

Family	Slice	Number of units	Length [m]	Strength [m^{-2}] $b_2 = \frac{B'}{B\rho}$	Quadrupole field B' [T/m]
QF	–	104	0.1500	4.0301	40.329
QFm	–	52	0.1500	3.7740	37.766
QFend	–	26	0.2500	3.6538	36.564
QDend	–	26	0.2500	−2.5037	−25.054
QDIP	QDf5	130	0.0500	−0.0001	−0.001
	QDf4	130	0.0500	0.0118	0.118
	QDf3	130	0.0500	−0.5529	−5.533
	QDf2	130	0.0500	−0.8678	−8.684
	QDf1	130	0.0500	−0.8666	−8.672
	QD0	130	0.3619	−0.8666	−8.672
QDIPm	QDs6	26	0.0500	0.0066	0.066
	QDs5	26	0.0500	−0.2720	−2.722
	QDs4	26	0.0500	−0.4260	−4.263
	QDs3	26	0.0500	−0.4269	−4.272
	QDs2	26	0.0500	−0.5861	−5.865
	QDs1	26	0.0500	−0.8721	−8.727
	QDs0	26	0.2042	−0.8724	−8.731
	QDm1	26	0.0500	−0.8725	−8.731
	QDm2	26	0.0500	−0.8737	−8.743
	QDm3	26	0.0500	−0.5567	−5.571
	QDm4	26	0.0500	0.0119	0.119
	QDm5	26	0.0500	−0.0001	−0.001

Table 3.6. Main parameters for the four quadrupole families and the gradient field integrated to dipoles of the M13-MX storage ring.

Family	Number of units	Length [m]	Strength [m^{-2}] $b_2 = \frac{B'}{B\rho}$	Quadrupole field B' [T/m]
Integrated to dipole	48	1.3739	−0.5772	−5.776
QD1	12	0.2295	−1.7745	−17.757
QD2	12	0.2891	−1.9373	−19.386
QD3	24	0.2892	−1.7573	−17.585
QF1	12	0.2902	1.5714	15.725
QF2	12	0.2891	1.8467	18.480
QF3	12	0.2901	1.6412	16.423
QF4	12	0.2299	1.3997	14.006
QF5	12	0.3096	1.7973	17.986
QF6	12	0.5277	2.0906	20.921
QF7	24	0.5282	2.0073	20.087
QF8	24	0.3088	2.0063	20.077

Table 3.7. Main parameters for the eleven quadrupole families of the A24-MX storage ring, the quadrupole field integrated to dipole is also included.

Family	Slice	Number of units	Length [m]	Strength [m^{-2}] $b_2 = \frac{B'}{B\rho}$	Quadrupole field B' [T/m]
QF	–	120	0.1500	4.0300	40.329
QFm	–	60	0.1500	3.7740	37.766
QFend	–	30	0.2500	3.6538	36.564
QDend	–	30	0.2500	−2.5037	−25.054
QDIP	QDf5	150	0.0500	−0.0001	−0.001
	QDf4	150	0.0500	0.0118	0.118
	QDf3	150	0.0500	−0.5551	−5.555
	QDf2	150	0.0500	−0.8713	−8.719
	QDf1	150	0.0500	−0.8701	−8.707
	QD0	150	0.3619	−0.8700	−8.706
QDIPm	QDs6	30	0.0500	0.0066	0.067
	QDs5	30	0.0500	−0.2731	−2.732
	QDs4	30	0.0500	−0.4277	−4.280
	QDs3	30	0.0500	−0.4286	−4.289
	QDs2	30	0.0500	−0.5884	−5.888
	QDs1	30	0.0500	−0.8756	−8.762
	QDs0	30	0.2042	−0.8759	−8.765
	QDm1	30	0.0500	−0.8760	−8.766
	QDm2	30	0.0500	−0.8771	−8.777
	QDm3	30	0.0500	−0.5589	−5.593
	QDm4	30	0.0500	0.0119	0.119
	QDm5	30	0.0500	−0.0001	−0.001

Table 3.8. Main parameters for the four quadrupole families and the gradient field integrated to dipoles of the M15-MX storage ring.

to meet the specific requirements of the insertion devices and the radio-frequency and injection systems of each basic designs. The lattice functions are matched as close as possible to the original ones by varying the quadrupole strengths using the MAD-X program. In the case of the M13-MX and M15-MX lattices this is very easy, since their beta functions do not change significantly after modify the bending angles of the dipoles. However, the beta functions of the A20-MX and A24-MX lattices present dramatic changes after modifying dipoles, so to get the desired beta functions, the matching process was more complicated. As a result, some quadrupole strength configurations were obtained, however, in this report only the solution with the best dynamic aperture is presented. It is worth mentioning that the quadrupole configurations with the best dynamic aperture are those with the smallest changes from their original settings, in all cases; for example, for the lattice A20-MX the best solution is one in which only the gradient field of dipoles is modified. The optical functions of the new lattices are shown in Figures 3.1-3.4, according to the OPA calculations, while the corresponding values of quadrupole strengths are given in Tables 3.5-3.8, of course, these values also give the correct working point (see next the Section).

3.1 Working Point Correction

In most cases it was necessary to change the working point, because it fell on or very near a resonance, or because the dynamic aperture was not good. Because theoretically there is no general criterion to get the working point with the optimal dynamic aperture, one has to resort to sophisticated computational methods to simulate the beam dynamics of lattices; the implementation of these computational methods is highly demanding in time and equipment, and it is beyond the current goals of this work. However, the criterion for changing the operating point should not be completely arbitrary, in this work a simple approach, but also very naive, is implemented, which consists of choosing points on the resonance diagram of lattice that are far from higher order resonances (fourth, fifth, sixth, ...), with the help of OPA. In addition, the new operating points should not being away from the initial point, in order to that through small changes in the quadrupole settings these points can be obtained. Several working points (at least two) were selected for each storage ring, and then, I chose which yield the largest dynamic aperture.

The procedure to correct the operating point depends on the basic design. For the A20-MX and A24-MX lattices, the most economical method is to find the most efficient pair of focusing and defocusing quadrupoles (QFi, QFj) which corrects the operating point, i.e., the pair that leads to desired tunes and that introduces the smallest changes to beta functions. This way, the lattice functions need not be matched again to their previous values. After trying all possible combinations was found that the most efficient pair is formed by the QD3 and QF7 families, in both cases. In the case of MAX IV based designs the situation is slightly different, the 7BA cell is designed such that to move the tunes suitably small variations in the strengths of families QD and QF are sufficient. To change the working point of the M15-MX and M13-MX lattices these variations were less than 0.6%, being so small the changes in the quadrupoles, QF and QD, the beta functions changed insignificantly. The quadrupoles values shown in Tables 3.5-3.8 give the final working points, which are shown in Figures 3.1.1 and 3.1.2.

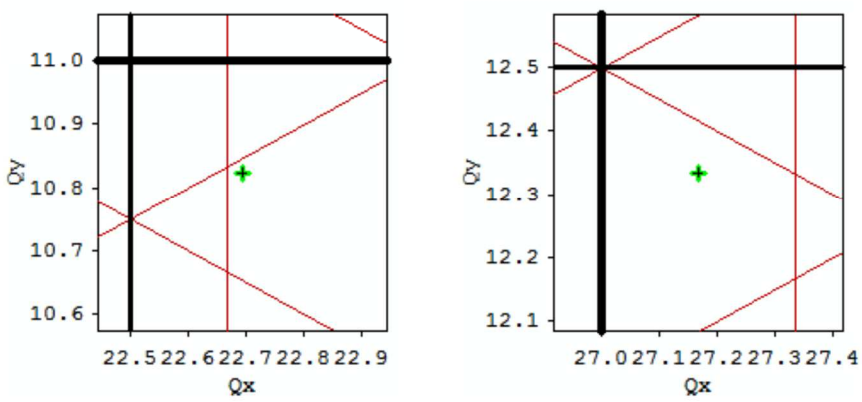

Figure 3.1.1. *Left:* working point of the A20-MX storage ring bare lattice at tunes $\nu_x = 22.694$ and $\nu_y = 10.823$. *Right:* working point of the A24-MX storage ring bare lattice at tunes $\nu_x = 27.166$ and $\nu_y = 12.334$. Resonance lines have been included up to third order.

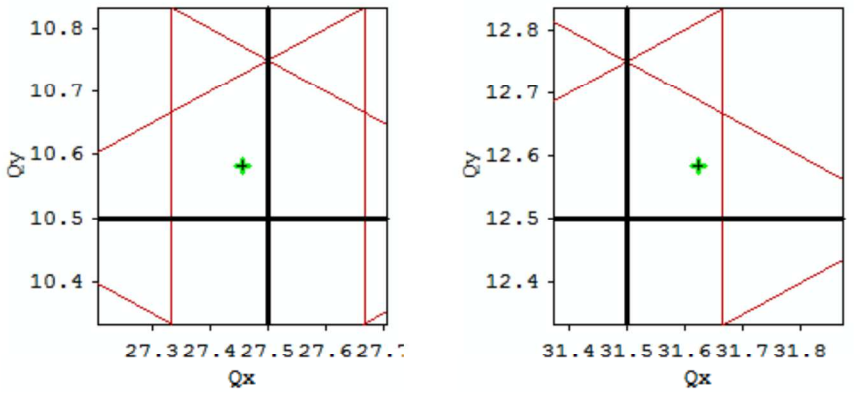

Figure 3.1.2. *Left:* working point of the M13-MX storage ring bare lattice at tunes $\nu_x = 27.456$ and $\nu_y = 10.582$. *Right:* working point of the M15-MX storage ring bare lattice at tunes $\nu_x = 31.624$ and $\nu_y = 12.584$. Resonance lines have been included up to third order.

3.2 Nonlinear Optics

A modern low-emittance synchrotron light source, as MAX IV and ALBA, is intrinsically nonlinear due to the strong sextupoles requiring its lattice, accordingly the nonlinear aspects must be addressed from the very beginning of the design. Inasmuch as the A20-MX, A24-MX, M13-MX and M15-MX lattices are based on cells of nonlinear designs already tested, the remaining task is to find sextupole strength configurations able to correct the undesirable nonlinear effects without that the dynamic aperture of lattices is reduced drastically. It is important to remember that the nonlinear lattice of MAX IV, unlike the ALBA case, includes octupoles to compensate the undesirable second order effects that introduce the intense sextupoles (see Section 2.3). However, in the current M13-MX and M15-MX lattices the octupoles of the original 7BA cell were not taken into account, their effects will be studied in a future work.

Family	Number of units	Length [m]	Strength [m^{-3}] $b_3 = \frac{1}{2}\frac{B''}{B\rho}$	$b_3 L$ [m^{-2}]	Sextupole field B'' [T/m^2]
SD1	10	0.1709	−26.21	−4.478	−524.5
SD2	10	0.1704	−15.81	−2.694	−316.4
SD3	10	0.1700	−52.01	−8.841	−1040.8
SD4	30	0.2408	−30.07	−7.240	−601.8
SD5	20	0.1699	−30.25	−5.140	−605.4
SF1	10	0.1730	12.47	2.157	249.6
SF2	10	0.2408	30.57	7.360	611.8
SF3	30	0.2407	32.36	7.789	647.7
SF4	20	0.1718	22.39	3.847	448.1

Table 3.2.1. Sextupole parameters of the A20-MX storage ring after the chromaticity correction and the dynamic aperture optimization using OPA.

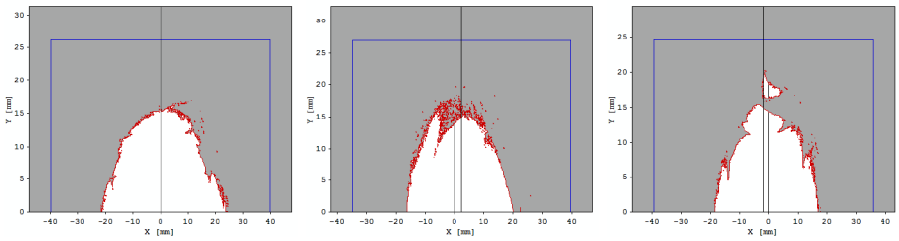

Figure 3.2.1. Dynamic aperture at the start ($s = 0$) of the A20-MX storage ring bare lattice (i.e. error free). From left to right: for on-momentum particles $\delta p/p = 0.0\%$, and for off-momentum particles $\delta p/p = 2.0\%$ and $\delta p/p = -2.0\%$.

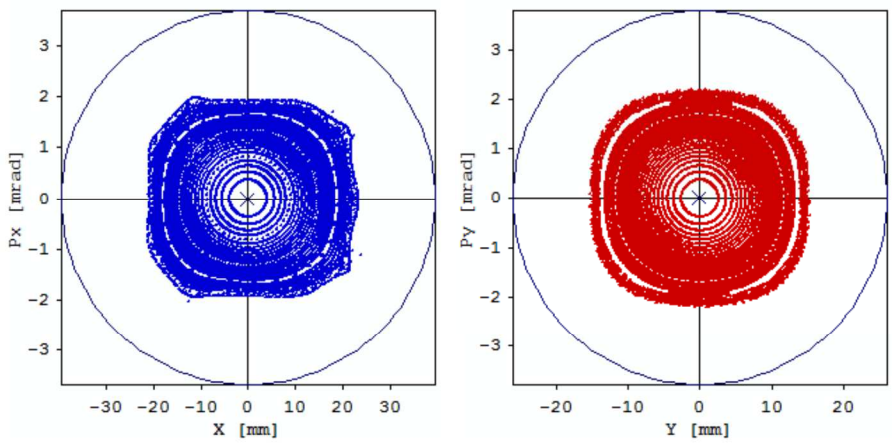

Figure 3.2.2. Poincare plots of the particle motion in horizontal (left) and vertical (right) phase spaces at the start ($s = 0$) of the A20-MX storage ring and with $\delta p/p = 0.0\%$, the tracking was performed with OPA in 2D. Although the axis are labeled with (x, p_x) and (y, p_y), in fact, the plots correspond to (x, x') and (y, y').

Family	Number of units	Length [m]	Strength [m^{-3}] $b_3 = \frac{1}{2}\frac{B''}{B\rho}$	$b_3 L$ [m^{-2}]	Sextupole field B'' [T/m^2]
SD1	12	0.1709	−36.39	−6.217	−728.2
SD2	12	0.1704	−18.82	−3.207	−376.6
SD3	12	0.1700	−58.36	−9.922	−1168.1
SD4	36	0.2408	−35.31	−8.501	−706.6
SD5	24	0.1699	−38.02	−6.460	−760.9
SF1	12	0.1730	15.55	2.689	311.2
SF2	12	0.2408	35.50	8.546	710.4
SF3	36	0.2407	40.40	9.725	808.6
SF4	24	0.1718	25.99	4.466	520.2

Table 3.2.2. Sextupole parameters of the A24-MX storage ring after the chromaticity correction and the dynamic aperture optimization using OPA.

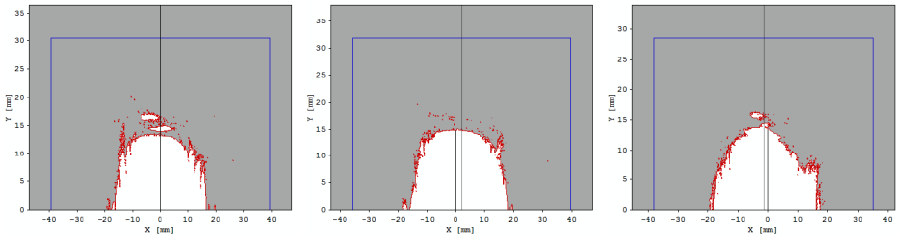

Figure 3.2.3. Dynamic aperture at the start ($s = 0$) of the A24-MX storage ring bare lattice (i.e. error free). From left to right: for on-momentum particles $\delta p/p = 0.0\%$, and for off-momentum particles $\delta p/p = 2.0\%$ and $\delta p/p = -2.0\%$.

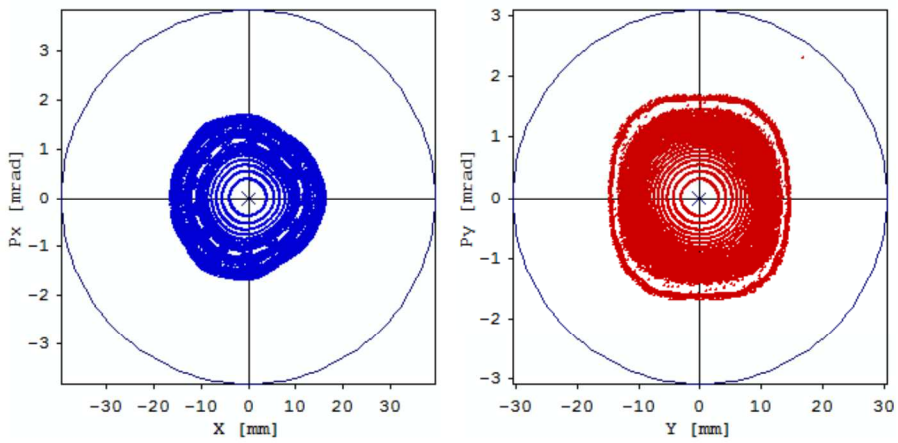

Figure 3.2.4. Poincare plots of the particle motion in horizontal (left) and vertical (right) phase spaces at the start ($s = 0$) of the A24-MX storage ring and with $\delta p/p = 0.0\%$, the tracking was performed with OPA in 2D. Although the axis are labeled with (x, p_x) and (y, p_y), in fact, the plots correspond to (x, x') and (y, y').

The sextupoles are introduced into linear lattices to correct the horizontal and vertical chromaticities, also called natural chromaticities, *in principle* only two families are necessary, but these sextupoles introduce nonlinear effects that can significantly reduce the dynamic aperture and therefore must be correct by additional sextupole families. Based on this, usually a procedure is established to correct the chromaticity and optimize the dynamic aperture simultaneously, which consists in to choose a pair of focusing and defocusing sextupoles to correct the chromaticity and the remaining sextupoles are used to optimize the dynamic aperture; after trying all possible combinations the pair demonstrating the longest dynamic aperture is fixed, and subsequent refinements to further increase the lattice dynamic aperture are carried out. This method is simple and usually works, as in the case of the lattices based on MAX IV design, however, for the A20-MX and A24-MX lattices were not obtained the desired results. In the latter case, the OPA program was used more intensively to find the results shown here.

For the A20-MX and A24-MX storage rings the horizontal and vertical natural chromaticities are given by

$$\xi_x^{\mathrm{n}}(\text{A20-MX}) = -49.82\,, \qquad \xi_x^{\mathrm{n}}(\text{A24-MX}) = -57.18\,,$$
$$\xi_y^{\mathrm{n}}(\text{A20-MX}) = -33.48\,, \qquad \xi_y^{\mathrm{n}}(\text{A24-MX}) = -36.76\,.$$

With the help of OPA to correct the natural chromaticities and optimize the dynamic aperture simultaneously[2], it was found that the sextupole strength configurations which provide the best solutions are those shown in Tables 3.2.1 and 3.2.2. Using these sextupole values, the chromaticities become small and positive,

$$\xi_x^{\mathrm{c}}(\text{A20-MX}) = 0.94\,, \qquad \xi_x^{\mathrm{c}}(\text{A24-MX}) = 1.06\,,$$
$$\xi_y^{\mathrm{c}}(\text{A20-MX}) = 0.79\,, \qquad \xi_y^{\mathrm{c}}(\text{A24-MX}) = 0.77\,,$$

and the dynamic aperture that is obtained for the A20-MX and A24-MX lattices is shown in Figures 3.2.1 and 3.2.3, respectively. The particle tracking for calculate the dynamic aperture was performed with OPA in two dimensions (2D) and, for on-momentum particles ($\delta p/p = 0\%$) and off-momentum particles ($\delta p/p = \pm 2.0\%$). Taking advantage of the facilities offered by OPA, Poincare plots were also calculated, the results are shown in Figures 3.2.2 and 3.2.4.

According to the original design of the MAX IV 7BA-cell, the SD and SFi sextupoles are the most efficient to correct the natural chromaticities, the other sextupole families (along with the octupoles) are intended to optimize the dynamic aperture. This remains true for the M13-MX and M15-MX storage rings, since their lattice functions do not vary significantly from those of the original design, only the dispersion is significantly increased. Therefore, the procedure described above can be applied quickly. Using the SD and SFi families, the natural chromaticities,

$$\xi_x^{\mathrm{n}}(\text{M13-MX}) = -32.42\,, \qquad \xi_x^{\mathrm{n}}(\text{M15-MX}) = -37.57\,,$$
$$\xi_y^{\mathrm{n}}(\text{M13-MX}) = -32.63\,, \qquad \xi_y^{\mathrm{n}}(\text{M15-MX}) = -37.00\,,$$

are compensated so that the corrected chromaticities are small and positive,

[2]Without applying the method described in the previous paragraph

Family	Number of units	Length [m]	Strength [m^{-3}] $b_3 = \frac{1}{2}\frac{B''}{B\rho}$	$b_3 L$ [m^{-2}]	Sextupole field B'' [T/m^2]
SD	130	0.1	-84.62	−8.462	−1693.6
SDend	26	0.1	-80.63	−8.063	−1613.7
SFm	26	0.1	33.50	3.350	670.5
SFo	26	0.1	174.00	17.400	3482.4
SFi	26	0.1	162.56	16.256	3253.5

Table 3.2.3. Sextupole parameters of the M13-MX storage ring after the chromaticity correction and the dynamic aperture optimization using OPA.

Family	Number of units	Length [m]	Strength [m^{-3}] $b_3 = \frac{1}{2}\frac{B''}{B\rho}$	$b_3 L$ [m^{-2}]	Sextupole field B'' [T/m^2]
SD	150	0.1	−93.62	-9.362	−1873.7
SDend	30	0.1	−113.59	-11.359	−2273.4
SFm	30	0.1	55.30	5.530	1106.8
SFo	30	0.1	174.00	17.400	3482.4
SFi	30	0.1	187.52	18.752	3753.0

Table 3.2.4. Sextupole parameters of the M15-MX storage ring after the chromaticity correction and the dynamic aperture optimization using OPA.

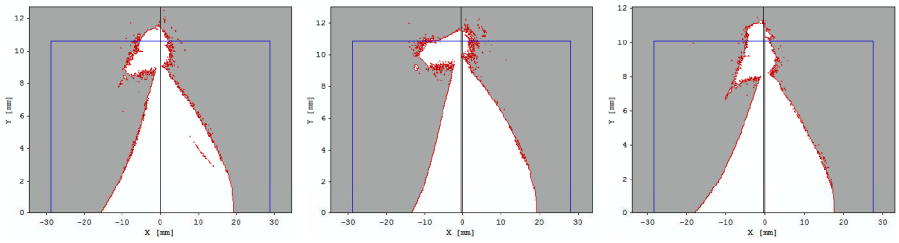

Figure 3.2.5. Dynamic aperture at the start ($s = 0$) of the M13-MX storage ring bare lattice (i.e. error free). The tracking was performed with OPA in 2D. From left to right: for on-momentum particles $\delta p/p = 0.0\%$, and for off-momentum particles $\delta p/p = 2.0\%$ and $\delta p/p = -2.0\%$.

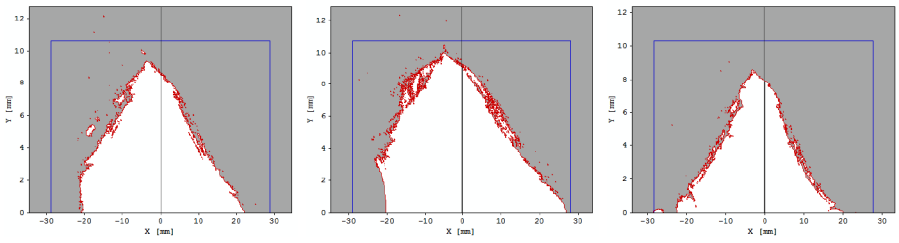

Figure 3.2.6. Dynamic aperture at the start ($s = 0$) of the M15-MX storage ring bare lattice (i.e. error free). The tracking was performed with OPA in 2D. From left to right: for on-momentum particles $\delta p/p = 0.0\%$, and for off-momentum particles $\delta p/p = 2.0\%$ and $\delta p/p = -2.0\%$.

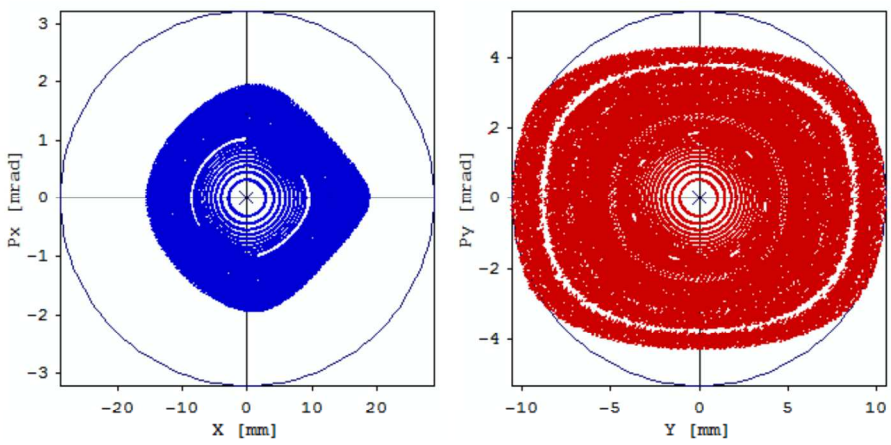

Figure 3.2.7. Poincare plots of the particle motion in horizontal (left) and vertical (right) phase spaces at the start ($s = 0$) of the M13-MX storage ring and with $\delta p/p = 0.0\%$, the tracking was performed with OPA in 2D. Although the axis are labeled with (x, p_x) and (y, p_y), in fact, the plots correspond to (x, x') and (y, y').

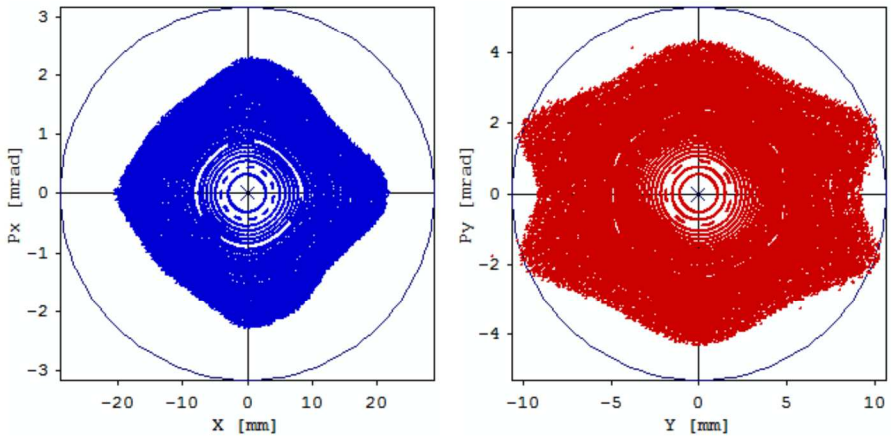

Figure 3.2.8 Poincare plots of the particle motion in horizontal (left) and vertical (right) phase spaces at the start ($s = 0$) of the M15-MX storage ring and with $\delta p/p = 0.0\%$, the tracking was performed with OPA in 2D. Although the axis are labeled with (x, p_x) and (y, p_y), in fact, the plots correspond to (x, x') and (y, y').

$$\xi_x^c(\text{M13-MX}) = 0.96\,, \qquad \xi_x^c(\text{M15-MX}) = 0.96\,,$$
$$\xi_y^c(\text{M13-MX}) = 1.00\,, \qquad \xi_y^c(\text{M15-MX}) = 1.00\,,$$

meantime the dynamic aperture is optimized with the SDend, SFm and SFo families. The final values, obtained with help of OPA, for the sextupoles are shown in Tables 3.2.3 and 3.2.4, and the resulting dynamic aperture for on-momentum particles ($\delta p/p = 0\%$) and off-momentum particles ($\delta p/p = \pm 2.0\%$) is shown in Figures 3.2.5 and 3.2.6; Figures 3.2.7 and 3.2.8 show the Poincare plots for the M13-MX and M15-MX lattices, respectively.

4 Discussion and Perspectives

After comparing the storage ring lattices of ALBA, DIAMOND II, ESRF II, MAX IV, NSLS II, SIRIUS and SOLEIL, the ALBA and MAXIV designs were chosen for carry out the studies presented here; which have the aim to give some feasible options for a medium energy storage ring of the Mexican synchrotron eventual. Besides their feasibility, the MAX IV and ALBA designs have two of the most important features that must be evaluated meticulously, because they are contrary in a some sense. On the one hand, MAX IV design offers a electron beam emittance very low, currently a feature in high demand by the synchrotron light users, but cost of its innovative technology is high, which could pose a budgetary problem for the Mexican project. And on the other hand, ALBA design is a cheaper option, but the resulting emittance is almost twice as large. Another important feature in a 3^{rd} generation synchrotron is the amount of free straight sections having the storage ring, where among other things the insertion devices are installed to provide high brightness light to users. In this matter the ALBA design is better, since 36% of the storage ring is of free straight sections, against 28% that offers the MAX IV design.

In summary, using a 7BA cell such as of the MAX IV facility, I obtain two storage rings, one with 396 m circumference and a horizontal emittance of 0.78 nm·rad, and other with 343.2 m circumference and a horizontal emittance of 1.2 nm·rad; and using a DBA cell such as of the ALBA facility, I obtain other two storage rings with circumferences of 403.2 and 336 m and horizontal emittances of 1.3 and 2.3 nm·rad, respectively. In all cases the beam energy has fixed to 3 GeV, which is the currently value of the ALBA and MAX IV facilities.

Although the studies were conducted at linear optics level, due to nonlinear nature of the low-emittance light sources, it was necessary make a superficial analysis of nonlinear optics of the lattices. As a result, all lattices obtained have acceptable dynamic aperture. However, a more thorough study of nonlinear aspects are mandatory, in particular, in the case of the M13-MX and M15-MX lattices is necessary include the original 7BA-cell octupoles. In addition, the nonlinear effects that are inherent to any physical lattice must be also considered, such as lattice errors due to misalignments, magnet fringe fields, etc., in order to obtain a robust dynamic aperture.

Studies on nonlinear dynamics of the A20-MX, A24-MX, M13-MX and M15-MX lattices are left for a future work. Where will also be conducted studies to improve the ALBA lattice design, this has a twofold purpose, on the one hand, to reduce the emittance of the A20-MX and A24-MX lattices, and on the other, to lay the groundwork for a possible update of the current ALBA facility. In this regard, is worth mentioning that a first attempt for reduce the emittance of the A20-MX and A24-MX lattices was done, unfortunately the results obtained are not satisfactory, only a 6% reduction of the horizontal emittance was obtained using permanent dipoles in the unit cells (as in the case of SIRIUS), reason for which are not in this present report.

5 Acknowledgments

This work was done during my stay in the accelerators group of the ALBA synchrotron (beam dynamics section), at all times I counted with the valuable

help of the group members, particularly of U. Iriso, Z. Martí and G. Benedetti. I thank the MINECO (Ministerio de Economía y Competitividad de España) by financial support.

References

[1] A. Antillón *at el.*, *Desarrollo de la Tecnología de Aceleradores: Fuente de Luz de Sincrotrón*, D.F., México, 2007.

[2] A. Antillón *at el.*, *Laboratorio Nacional de Aceleradores y Luz Sincrotrón*, D.F., México, 20011.

[3] G. Contreras *at el.*, *Línea de luz Sincrotrón en México: Acelerador lineal de electrones*, D.F., México, 2012.

[4] J. Ablett *et al.*, *NSLS-II Conceptual Design Report*, December 2006, Brookhaven National Laboratory.

[5] *NSLS-II Source Properties and Floor Layout*, Abril 2010, http://www.bnl.gov/ps/docs/pdf/SourceProperties.pdf

[6] A. Rodrigues *et al.*, *Sirius Design Report*, February 2013, Laboratório Nacional de Luz Síncrotron.

[7] L. Lin, *Design challenges in Sirius*, 3rd Low Emittance Ring Workshop (2013), Oxford, U. K.

[8] *Detailed Design Report on the Max IV Facility*, August 2010, https://www.maxlab.lu.se/node/1136

[9] http://www.esrf.eu/Accelerators/Accelerators/StorageRing

[10] J.-L. Revol *et al.*, Proc. IPAC 2013, Shanghai, China, pp. 82-84.

[11] L. Farvacque *et al.*, Proc. IPAC 2013, Shanghai, China, pp. 79-81.

[12] J.-L. Revol *et al.*, Proc. IPAC 2013, Shanghai, China, pp. 1140-1142.

[13] V. P. Suller, Proc. EPAC 2002, Paris, France, pp. 757-759.

[14] R. P. Walker, Proc. PAC 2003, Portland, Oregon, U.S., pp. 232-234.

[15] R. Bartolini *et al.*, Proc. IPAC 2013, Shanghai, China, pp. 240-242.

[16] R. Bartolini *et al.*, *A DDBA lattice upgrade of the Diamond ring*, 3rd Low Emittance Ring Workshop (2013), Oxford, U. K.

[17] R. Nagaoka *et al.*, Proc. IPAC 2013, Shanghai, China, pp. 76-78.

[18] A. Nadji *et al.*, Proc. IPAC 2013, Shanghai, China, pp. 73-75.

[19] M. Muñoz and D. Einfeld, Proc. PAC 2005, Knoxville, Tennessee, pp. 3777-3779.

[20] D. Einfeld, E. Levichev and P. Piminov, Proc. EPAC 2008, Genoa, Italy, pp. 3140-3142.

[21] M. Pont, *Magnets for Accelerators: The Alba case*, talk for operators training, March 2013.